Ising model on finite projective geometries

Bachelor's Thesis in Physics

Presented by

Kai Klede

June 29, 2018

Institut für Theoretische Physik
Friedrich-Alexander-Universität Erlangen-Nürnberg

Supervisor:
Prof. Dr. Klaus Mecke

Abstract

This thesis investigates the nearest neighbor Ising Model on two dimensional finite projective spaces, over finite fields of prime order. The neighborhood relation is defined by a flat biquadric field. When spins are placed only in the affine plane, the mean field critical exponents are found numerically via finite size scaling. The interpretation of these results suggests a notion of system size, proportional to the square root of the field order. The graph diameter as candidate for this system size is ruled out. A high temperature expansion of fifth order was not sufficient to extract the critical behavior analytically.

When spins are placed everywhere on the projective space, simulation indicates that the line at infinity and the affine plane cannot be treated separately, but have to be considered as a whole.

Contents

1 Introduction

100 years ago, the formulation of general relativity revolutionized our understanding of physics. The predictions made by Einstein's theory agree with experimental observation incredibly well. At its core, general relativity is a theory of geometry. It describes spacetime as a four-dimensional differentiable manifold, equipped with a metric tensor, that generalizes the scalar product in Euclidean geometry and defines a notion of length.

Quantum field theory is the predominant theory of physics at small scales. Like general relativity, it has been verified in numerous experiments. In situations, where both gravitation and quantum effects are relevant, problems emerge when trying to combine these theories. Due to them being conceptually completely different in nature, various attempts to reconcile both theories haven't yet led to a breakthrough in the construction of a unified theory of quantum gravitation.

A fundamentally new approach has been brought forward by Prof. Dr. Mecke in "Biquadrics configure finite projective geometry into a quantum spacetime" [17]. Instead of starting from the formerly mentioned theories, the idea is to conceptually embed quantum nature in a completely new description of geometry. A promising candidate for an inherently finite spacetime are finite projective spaces. A biquadric field will play the role of the metric tensor in general relativity and define a notion of distance on these spaces (both terms will be defined rigorously in section 2).

The fundamental nature of this approach requires revisiting various concepts of physics. The field of statistical physics on lattice models is of particular interest, because like gravity, it is closely related with geometry. A change of the underlying geometry will entail changes in the behavior of statistical systems. Conversely, from the behavior of statistical systems, conclusions can be drawn about their underlying geometry.

This thesis focuses on analyzing statistical physics on finite projective geometries. Exemplary, the nearest neighbor Ising model is studied, because of its sensitive dependence on the topology of the lattice and because it is one of the most widely used and best understood models in statistical physics.

2 Finite projective geometry

2.1 Finite projective space $\mathfrak{P}\mathbb{K}_p^d$

A d-dimensional projective space $\mathfrak{P}\mathbb{K}^d$ over a field $\mathbb{K}$ can be constructed by projection of a $(d+1)$-dimensional $\mathbb{K}$-vectorspace V. It can be thought of as the geometry whose *points* are identified with the one-dimensional subspaces of V, whose *lines* can be identified as the two-dimensional subspaces of V and so forth [6].

Any $(d+1)$-dimensional $\mathbb{K}$-vectorspace is isomorphic to $\mathbb{K}^{d+1}$, so choose V to be $\mathbb{K}^{d+1}$ as convention. We define the binary equivalence relation $\sim$:

Definition 2.1. For $x, y \in \mathbb{K}^{d+1}$: $\quad x \sim y \iff \exists \lambda \in \mathbb{K}^\times$ such that $\lambda x = y$

Definition 2.2. The *d-dimensional projective space* is then defined as the point set $\mathfrak{P}\mathbb{K}^d := \left(\mathbb{K}^{d+1} \setminus \{0\}\right) / \sim$.

Definition 2.3. The *n-dimensional affine subspace* of $\mathbb{K}^{d+1}$ is denoted

$$\mathfrak{A}\mathbb{K}^n := \{e_{n+1} + x \mid x \in \operatorname{span}\{e_1, \ldots, e_n\}\} \tag{1}$$

where $(e_i)_{i\in\{1,\ldots,d+1\}}$ is an ordered basis of $\mathbb{K}^{d+1}$, $n \in \mathbb{N}_0$ and $n \leq d$.

Definition 2.4. The section $s : \mathfrak{P}\mathbb{K}^d \to \mathbb{K}^{d+1}$ maps a point in the projective space to a point in the embedding vectorspace via

$$s := \iota \circ \tilde{s} \tag{2}$$

with $\iota : \dot{\bigcup}_{n=0}^{d} \mathfrak{A}\mathbb{K}^n \to \mathbb{K}^{d+1}$ the inclusion and $\tilde{s} : \mathfrak{P}\mathbb{K}^d \to \dot{\bigcup}_{n=0}^{d} \mathfrak{A}\mathbb{K}^n$,

$$\tilde{s} : [y] \mapsto x \in \dot{\bigcup}_{n=0}^{d} \mathfrak{A}\mathbb{K}^n \text{ such that } y \sim \iota(x) \tag{3}$$

$\tilde{s}$ is well defined, because each equivalence class intersects exactly one affine subspace in a unique point.

Definition 2.5. Any point in $\mathfrak{P}\mathbb{K}^d$ can be assigned the coordinates of its image point under s with respect to $(e_i)_{i\in\{1,\ldots,d+1\}}$. These coordinates are called *homogeneous coordinates* and will be denoted in angular brackets.

Definition 2.6. The *line* spanned by two points $x, y \in \mathfrak{P}\mathbb{K}^d$ is defined as

$$\left\{z \in \mathfrak{P}\mathbb{K}^d \mid \exists \lambda, \mu \in \mathbb{K} \text{ with } \lambda \neq 0 \text{ or } \mu \neq 0 \text{ such that } s(z) = \lambda s(x) + \mu s(y)\right\} \tag{4}$$

Motivated by the above construction, one can generalize the notion of projective space for dimensions ≥ 3, as shown by Veblen and Young [20][21].

Theorem 2.7. *Let X be a set of points, $\mathscr{L}$ a set of subsets of X called lines, satisfying*

(a) any two points lie on a unique line

(b) a line meeting two sides of a triangle, not at a vertex, meets the third side

(c) a line contains at least three points

Then X and $\mathscr{L}$ are the sets of points and lines in a projective space of dimension ≥ 3.

An illustration of the duality between the axiomatic characterization of projective spaces and the description with an embedding subspace is Figure 1.

In this thesis we will focus on *finite projective spaces*.

Definition 2.8. A projective space $\mathfrak{P}\mathbb{K}^d$ over a finite field $\mathbb{K}$ is called *finite*.

For finite fields, Galois' Theorem [6] states

Theorem 2.9. *A finite field has prime power order. For any prime power $q = p^n$, where p prime, $n \in \mathbb{N}$, there is a unique finite field of order q.*

Therefore it is meaningful to denote a d-dimensional finite projective space over a field of order q as $\mathfrak{P}\mathbb{K}_q^d$. In the following we will restrict ourselves to the case where $q = p$ is prime, in order to be able to construct the biquadrics in the next section.

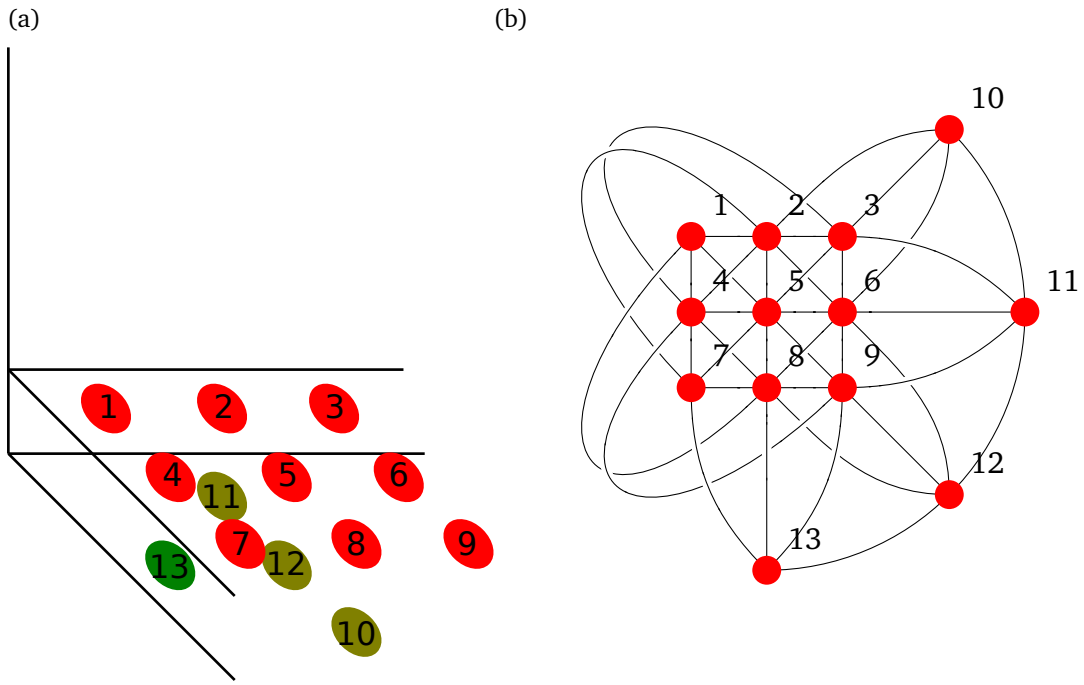

Figure 1: Figure a) marks the points in $\mathbb{K}^{d+1}$ that can be identified with the points in $\mathfrak{P}\mathbb{K}_3^2$. Figure b) shows the same space $\mathfrak{P}\mathbb{K}_3^2$, but represented as points and lines.

2.2 Neighborhood defined by biquadrics

One caveat in modeling spacetime as finite projective space is the lack of a metric. This issue is addressed by defining a notion of distance, and in particular a set of nearest neighbors. This is achieved by introducing the analog of a cone section in the finite projective space.

This approach is motivated by the definition of the metric tensor in general relativity, which is essentially a non-degenerate symmetric bilinear form on each tangent space of spacetime. This idea was first brought forward by Mecke [17].

Definition 2.10. A *quadric* is the set of points

$$Q \coloneqq \{[q] \in \mathfrak{P}\mathbb{K}_p^d \mid (q,q) = 0\} \tag{5}$$

Where $(\cdot,\cdot) : \mathbb{K}^{d+1} \times \mathbb{K}^{d+1} \to \mathbb{K}$ denotes a non-degenerate symmetric bilinear form. This is well-defied, because for any $q, \tilde{q} \in \mathbb{K}^{d+1}$ such that $q \sim \tilde{q}$ and $(q,q) = 0$, there exists a $\lambda \in \mathbb{K}^\times$, such that

$$(\tilde{q},\tilde{q}) = (\lambda q, \lambda q) = \lambda^2 (q,q) = 0 \tag{6}$$

The corresponding matrix to the bilinear form in homogeneous coordinates is denoted $\hat{Q}$.

Definition 2.11. A point $\hat{c} \notin Q$ is called *center* of a quadric Q, if any line that intersects the center and a quadric point, also intersects a second quadric point.

Note that such a center is not uniquely determined. The definition of the center simultaneously distinguishes a dual *hyperplane at infinity*.

Definition 2.12. The *hyperplane at infinity* with respect to a quadric Q and a center $\hat{c}$ is the set

$$H_{\hat{c}}^\infty = \left\{ x \in \mathfrak{P}\mathbb{K}_p^d \mid (x,c) = 0 \right\} \tag{7}$$

with its *normal vector* $\hat{h}_{\hat{c}}^\infty \coloneqq \hat{c}^{\mathrm{T}} \hat{Q}$.

As pointed out earlier, the center is not uniquely defined by a quadric. Thus in the following, the center $\hat{c} = \langle 0, \ldots, 1 \rangle^{\mathrm{T}} \in \mathfrak{P}\mathbb{K}_p^d$ is chosen. With this choice, the matrix $\hat{Q}$ can be normalized to the form

$$\hat{Q} = \begin{pmatrix} \mathbf{G}_d & \vec{0} \\ \vec{0}^{\mathrm{T}} & -1 \end{pmatrix} \tag{8}$$

The block matrix $\mathbf{G}_d$ is called a *pre-metric*. Note that $\mathfrak{P}\mathbb{K}_p^d \setminus H_{\hat{c}}^\infty$ can be identified with $\mathfrak{A}\mathbb{K}^d$, similarly to Definition 2.5.

However, even with a fixed choice of center, not any line passing through the center also intersects the quadric. A remedy to that problem is the introduction of a second complementary quadric to a given quadric and center point. For simplicity, we stick to the above choices for the following definition of a *biquadric*.

Definition 2.13. The *biquadric* $Q_0^{\pm}$ with center $\hat{c} = \langle 0, \dots, 1 \rangle^{\mathrm{T}} \in \mathfrak{P}\mathbb{K}_p^d$ is the union of the quadrics Q_0^+ and Q_0^- given by the bilinear forms

$$\hat{Q}_0^+ = \begin{pmatrix} \mathbf{G}_d^+ & \vec{0} \\ \vec{0}^{\mathrm{T}} & {f_+}^2 \end{pmatrix} \quad \hat{Q}_0^- = \begin{pmatrix} \mathbf{G}_d^- & \vec{0} \\ \vec{0}^{\mathrm{T}} & -{f_-}^2 \end{pmatrix} \tag{9}$$

with $f_\pm \in \mathbb{K}_q$, the *spatial scaling factor* $f := \frac{f_-}{f_+}$, where $-f_-^2$ must be a non-square.

The biquadric $\hat{Q}_0^\pm$ can always be rescaled such that ${f_+}^2 = 1$. In this thesis we will exclusively consider spatially isotropic biquadrics and therefore require $\mathbf{G}_d^+ = \mathbf{G}_d^- =: \mathbf{G}_d$

Definition 2.14. Given a biquadric with a center, the points in the biquadric are called *neighbors* of the center point.

The choice of the pre-metric $\mathbf{G}_d$ can further be narrowed down by a classification of isomorphic quadrics. Such a complete classification for quadrics over finite fields in d dimensions is given in [10]. For the work in this thesis, the following results are sufficient.

In real vectorspaces Sylvester's law of inertia states that for $\hat{A}$ the matrix of a quadric and any invertible S, such that $D = S^{\mathrm{T}}\hat{A}S$ is diagonal, the number of negative elements in D is the same for all such S. The signature of the matrix of a real quadric is invariant under change of basis. For finite fields $\mathbb{K}_p$, this is not the case. If $p \equiv 3 \mod 4$, the equation $a^2 + b^2 = -1$ has solutions and there exists an invertible matrix $\mathbf{P}$, such that

$$\begin{pmatrix} -1 & 0 \\ 0 & -1 \end{pmatrix} = \mathbf{P}^{\mathrm{T}} \begin{pmatrix} 1 & 0 \\ 0 & 1 \end{pmatrix} \mathbf{P} \tag{10}$$

with

$$\mathbf{P} = \begin{pmatrix} a & b \\ -b & a \end{pmatrix} \quad \mathbf{P}^{-1} = -\mathbf{P}^{\mathrm{T}} \tag{11}$$

An implication of this is that in even dimensions d, all quadrics Q are equivalent, i.e. one can always find an invertible S, such that $S^{\mathrm{T}}\hat{Q}S = \mathbb{1}_{\mathbf{d+1}}$.

However, biquadrics have to be transformed simultaneously. There are two canonical forms of non-degenerate biquadrics $Q_0^\pm$. They are distinguished by their pre-metric and are called Minkowskian or Euclidean, according to their signature, corresponding to either the one of the scalar product in Euclidean geometry, or the signature of the pseudo metric in Minkowskian spacetime.

$$\mathbf{G}_{\text{Minkowski}} := \begin{pmatrix} -1 & \vec{0} \\ \vec{0}^{\mathrm{T}} & \mathbb{1}_{d-1} \end{pmatrix} \quad \mathbf{G}_{\text{Euclid}} := \begin{pmatrix} 1 & \vec{0} \\ \vec{0}^{\mathrm{T}} & \mathbb{1}_{d-1} \end{pmatrix} \tag{12}$$

So far we have only considered the biquadric centered at $\langle 0, \dots, 0, 1 \rangle^{\mathrm{T}}$. To obtain a biquadric centered at any point $\hat{c} \in \mathfrak{A}\mathbb{K}^d \subset \mathfrak{P}\mathbb{K}_p^d$ we apply a transformation to $Q_0^\pm$ that maps $\langle 0, \dots, 0, 1 \rangle^{\mathrm{T}} \mapsto \hat{c}$.

With the help of a biquadric, we defined local neighborhood relative to a center (Definition 2.14). In order to define a local neighborhood for any point, we equip every point with a biquadric, a so called *biquadric field*.

We require neighborhood to be symmetric, and formulate the following *dynamical constraint* for biquadrics:

$$\hat{c} \in Q^{\pm}(\hat{q}) \text{ if and only if } \hat{q} \in Q^{\pm}(\hat{c}) \tag{13}$$

Because $\hat{Q}$ is bilinear, if $\hat{q} \in Q$, then also $-\hat{q} \in Q$ and therefore a simple solution that satisfies this constraint is the *flat space*

$$\mathfrak{SK}_p^d = \left(\mathfrak{PK}_p^d, Q^{\pm}(\hat{p})\right) \tag{14}$$

with $Q^{\pm}(\hat{p})$ the translated version of $Q_0^{\pm}$, with the translation $T_{-\hat{p}}$ that maps $\hat{p}$ to $\langle 0, \ldots, 0, 1\rangle^{\mathrm{T}}$. In matrix notation

$$\hat{Q}^{\pm}(\hat{p}) = \hat{T}_{-\hat{p}}^{\mathrm{T}} \hat{Q}_0^{\pm} \hat{T}_{-\hat{p}} \tag{15}$$

$$\text{with } \hat{T}_{-\hat{p}} := \begin{pmatrix} 1 & 0 & \cdots & -\hat{p}_1 \\ 0 & 1 & & -\hat{p}_2 \\ \vdots & & \ddots & \vdots \\ 0 & 0 & \cdots & 1 \end{pmatrix} \tag{16}$$

2.3 Constructing solutions to two-dimensional biquadrics

In the course of this thesis, intensive computational analysis of the neighborhood structure, given by the biquadric fields is performed. Therefore, an efficient method to construct the solutions to a biquadric is needed. General approaches as developed in [27] are far too complicated. The specific structure of the biquadrics studied here, allows us to find all solutions in two-dimensions as follows:

$$\hat{q}_+ = \begin{pmatrix} 1 \\ 0 \\ 1 \end{pmatrix} \text{ and } \hat{q}_- = \begin{pmatrix} 0 \\ f \\ 1 \end{pmatrix} \tag{17}$$

are always affine solutions of the quadrics Q^+ and Q^- respectively.

$$\hat{Q}^+ = \begin{pmatrix} -1 & 0 & 0 \\ 0 & 1 & 0 \\ 0 & 0 & 1 \end{pmatrix} \text{ and } \hat{Q}^- = \begin{pmatrix} -1 & 0 & 0 \\ 0 & 1 & 0 \\ 0 & 0 & -f \end{pmatrix} \tag{18}$$

The other solutions $\hat{q}$ of this biquadric in the affine plane can be obtained by applying the transformations $\hat{q} = \Lambda(\alpha)\hat{q}_{\pm}$, with

$$\Lambda(\alpha) := \begin{pmatrix} \frac{\alpha+\alpha^{-1}}{2} & \frac{\alpha-\alpha^{-1}}{2} & 0 \\ \frac{\alpha-\alpha^{-1}}{2} & \frac{\alpha+\alpha^{-1}}{2} & 0 \\ 0 & 0 & 1 \end{pmatrix} \tag{19}$$

where $\alpha \in \mathbb{K}^\times$. These leave $\hat{Q}^\pm = \Lambda(\alpha)^\mathrm{T}\hat{Q}^\pm\Lambda(\alpha)$ invariant. So all $\hat{q} = \Lambda(\alpha)\hat{q}_\pm$ are solutions to the quadric. As shown in [17] the biquadric has $2\cdot(p-1)$ affine solutions and

$$\left|\left\{\left\langle \begin{smallmatrix} \frac{\alpha+\alpha^{-1}}{2} \\ \frac{\alpha-\alpha^{-1}}{2} \\ 1 \end{smallmatrix}\right\rangle, \left\langle \begin{smallmatrix} f\frac{\alpha-\alpha^{-1}}{2} \\ f\frac{\alpha+\alpha^{-1}}{2} \\ 1 \end{smallmatrix}\right\rangle \mid \alpha \in \mathbb{K}_p^\times\right\}\right| = 2\cdot\left|\mathbb{K}_p^\times\right| = 2\cdot(p-1) \tag{20}$$

So with $\hat{q} = \Lambda(\alpha)\hat{q}_\pm$ already all solutions to the biquadric are known.

In order to determine the multiplicative inverse α^{-1} in galois fields $\mathbb{K}_p$ of prime order, the identity

$$\alpha^{-1} \equiv \alpha^{p-2} \mod p \tag{21}$$

can be used. In the numerical computation, attention has to be paid to possible integer overflows for higher field orders. Therefore the algorithm described on page 244 of 'Applied Cryptography: Protocols, Algorithms, and Source Code in C' [24] is used in the implementation.

3 The Ising Model on finite projective spaces

In statistical physics, the Ising Model is used to describe the collective behavior of spin networks. In this thesis, although the terms spin, magnetic dipole moment, etc. are used, they are not meant in the literal sense that the finite projective geometry actually describes a physical lattice structure. We are more interested in the general behavior of Ising-like systems on projective geometry and whether the geometry induces some collective effects.

The traditional Ising Model consists in placing 'spins' on a hypercubic lattice in an external field. A 'spin' in the Ising Model is restricted to the external field axis and can evaluate to either $+1$ or -1. In its simplest form, the interaction between spins is limited to immediately adjacent sites (Nearest Neighbor Ising Model). The interaction Hamiltonian in this model is

$$\mathscr{H} = -h\sum_{i=1}^{n}\sigma_i - \sum_{<i,j>} J_{ij}\sigma_i\sigma_j \tag{22}$$

with the external field h, interaction constants J_{ij} and spins σ_i. $\sum_{<i,j>}$ denotes the sum over all adjacent spin-pairs σ_i and σ_j. In the following we will assume the same interaction strength for all neighbor pairs $J_{ij} = J$:

$$\mathscr{H} = -h\sum_{i=1}^{n}\sigma_i - J\sum_{<i,j>}\sigma_i\sigma_j \tag{23}$$

The canonical partition function is then defined as

$$\sum_{\omega} e^{-\beta\mathscr{H}(\omega)} \tag{24}$$

where $\sum_{\omega}$ denotes the sum over all microstates, i. e. all possible spin configurations of the system.

Historically, it took almost 20 years, after Ising published his solution to the one-dimensional case in 1925 [11], until Lars Onsager found an analytic solution to the two-dimensional case in 1944 [19]. The three-dimensional case is still an open problem today. In the following we will thus concentrate on the two-dimensional case for projective spaces, because the one-dimensional case is practically equivalent to the Ising Model on a hypercubic lattice.

In this thesis we focus on what we called flat spaces (Equation 14) with a Minkowskian biquadric field (Equation 12) in the previous section. Furthermore, two cases will be distinguished: One is placing spins on all points in the affine subspace $\mathfrak{A}\mathbb{K}^2$, while leaving the hyperplane at infinity unoccupied. The other consists in placing a spin on each point in the projective space. In both cases, the spin-spin interaction is restricted to neighboring spins, in the sense of Definition 2.14.

4 Exact results for low field orders

In order to evaluate the dependability of the numerical process, exact solutions are calculated for simple cases of low field orders.

In the case of a Euclidean premetric (see Equation 12) and spins on the affine plane only, the sum over all possible configurations ω can be reduced to a sum over all spins. The reason is that for $\mathfrak{PK}_2^2$ and $\mathfrak{PK}_3^2$, the neighbors of each point in the affine plane, are simply all the other points in the affine plane. For such a densely connected lattice, the field free partition function is:

$$Z = \sum_{\omega} e^{\beta \sum_{<i,j>} \sigma_i \sigma_j} = \sum_{i=0}^{n} \binom{n}{i} e^{\beta \cdot \left(\frac{n(n-1)}{2} - 2 \cdot i \cdot (n-i)\right)} \tag{25}$$

where n is the number of spins on the lattice.

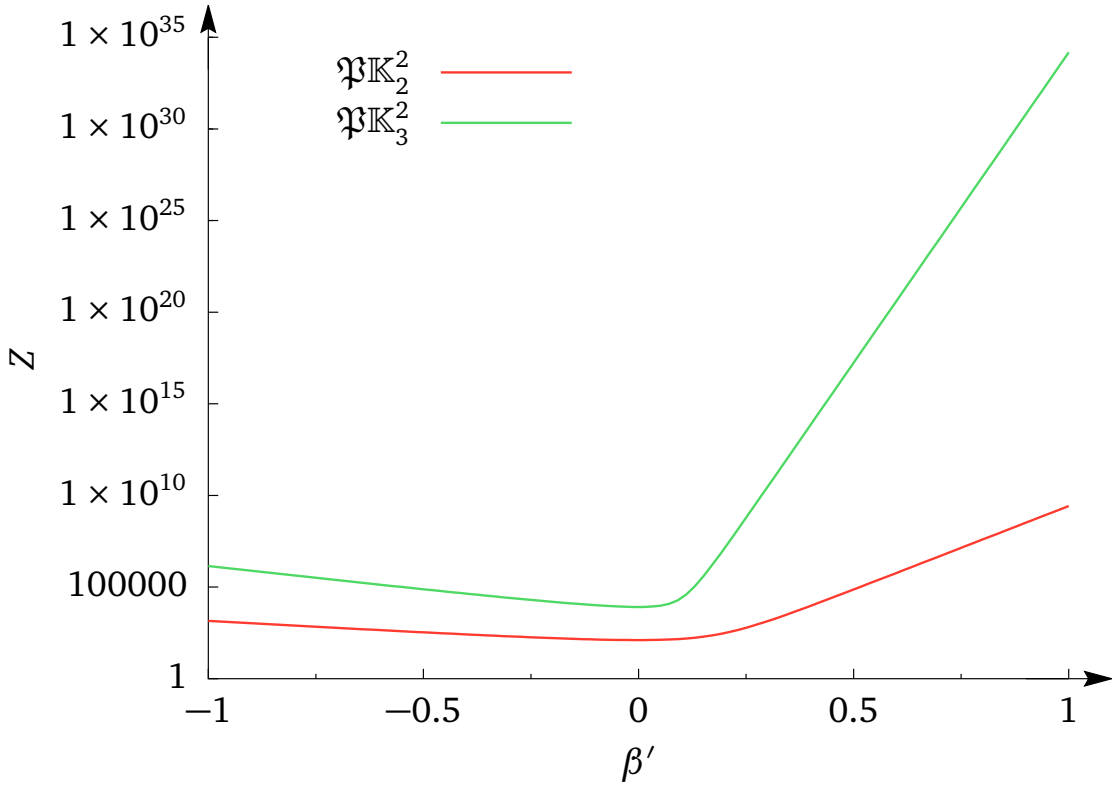

Figure 2: Exact partition function (25) for $\mathfrak{PK}_2^2$ and $\mathfrak{PK}_3^2$ with a Euclidean pre-metric.

More relevant for the comparison with simulation results, is the Minkowskian case. Here, exact results were obtained for $\mathfrak{PK}_3^2$ and $\mathfrak{PK}_5^2$ via direct execution of the sum over all configurations in the partition function (24). From the general partition function, other quantities like the specific heat C_h (Figure 9), or the Magnetization $M(\beta, h)$ (Figure 10), were derived for comparison with the numerical results.

5 Approximate theories

5.1 Mean field approximation

Instead of considering the interaction of a spin with all its neighbors, in the mean field approximation, an approximate interaction with an average spin is considered. This drastically simplifies the calculation of the partition function to a single spin problem.

By substituting σ_j by $\langle\sigma\rangle := \frac{1}{n}\sum_{i=1}^{n}\sigma_i$ the average over all spins in Equation 23, we obtain the following simplified Hamiltonian:

$$\mathscr{H} = -h\sum_{i=1}^{n}\sigma_i - J\langle\sigma\rangle\sum_{i=1}^{m}\sigma_i \tag{26}$$

m the total number of neighbor pairs. In the case with spins on the affine plane only, all spins have the same number of neighbors, so the Hamiltonian can be expressed as:

$$\mathscr{H} = -\underbrace{\left(h + \frac{J\nu}{2}\langle\sigma\rangle\right)}_{h_{\text{eff}}}\sum_{i=1}^{n}\sigma_i \tag{27}$$

where ν is the number of neighbors per spin. The partition function for the flat space is then

$$Z_{\text{MF}} = \sum_{i=0}^{n}\binom{n}{i}\exp\left(\beta\cdot\left(h + \frac{J\nu}{2}\langle\sigma\rangle\right)\cdot(n-2i)\right) \tag{28}$$

$$\overset{n \text{ uneven}}{=} \sum_{k=1}^{\frac{n-1}{2}}\binom{n}{2k+1}\cosh\left(\beta h_{\text{eff}}(2k+1)\langle\sigma\rangle\right) \tag{29}$$

The derivation of the magnetization yields a self consistency condition for $\langle\sigma\rangle$.

$$M = n\cdot\langle\sigma\rangle \tag{30}$$

$$M = -\frac{\partial F}{\partial h} = \frac{1}{\beta}\frac{\partial \ln Z_{\text{MF}}}{\partial h} \tag{31}$$

$$= \frac{\sum_{i=0}^{n} -(2i-n)\binom{n}{i}e^{-\beta(2i-n)\left(\frac{J\nu}{2}\langle\sigma\rangle+h\right)}}{\sum_{i=0}^{n}\binom{n}{i}e^{-\beta(2i-n)\left(\frac{J\nu}{2}\langle\sigma\rangle+h\right)}} \tag{32}$$

The solutions for the self consistency condition are calculated numerically via bisection. The results are depicted in Figure 3.

Furthermore the critical value for β can be derived analytically.

$$\frac{\partial M_{h=0,J=1}}{\partial\langle\sigma\rangle}\Big|_0 = \frac{\beta_{\text{crit}}\nu}{2}\left(\frac{\sum_{i=0}^{n}(2i-n)^2\binom{n}{i}}{\sum_{i=0}^{n}\binom{n}{i}} - \frac{\left(\sum_{i=0}^{n}(2i-n)\binom{n}{i}\right)^2}{\left(\sum_{i=0}^{n}\binom{n}{i}\right)^2}\right) \overset{!}{=} n \tag{33}$$

With the identities [4]

$$\sum_{i=1}^{n} i\binom{n}{i} = \sum_{i=1}^{n} i\frac{n!}{i!(n-i)!} = \sum_{i=1}^{n} n\frac{(n-1)!}{(i-1)!(n-i)!} = n\cdot 2^{n-1} \tag{34}$$

$$\sum_{i=1}^{n} i^2\binom{n}{i} = n\cdot(n+1)\cdot 2^{n-2} \tag{35}$$

it is straightforward to show, that Equation 33 becomes

$$n \overset{!}{=} \frac{\beta_{\text{crit}}\nu}{2}\left(\frac{2^n\cdot n}{2^n} - \frac{0^2}{2^{2n}}\right) \tag{36}$$

$$\beta_{\text{crit}} = \frac{2}{\nu} \tag{37}$$

As could be already seen from the mean field partition function (Equation 29), we expect the critical temperature to be proportional to the number of neighbors, which in turn is given by $2\cdot(p-1)$ in the affine, Minkowskian case. So from now on we denote

$$\beta' = \beta \ \cdot \text{ number of neighbors.} \tag{38}$$

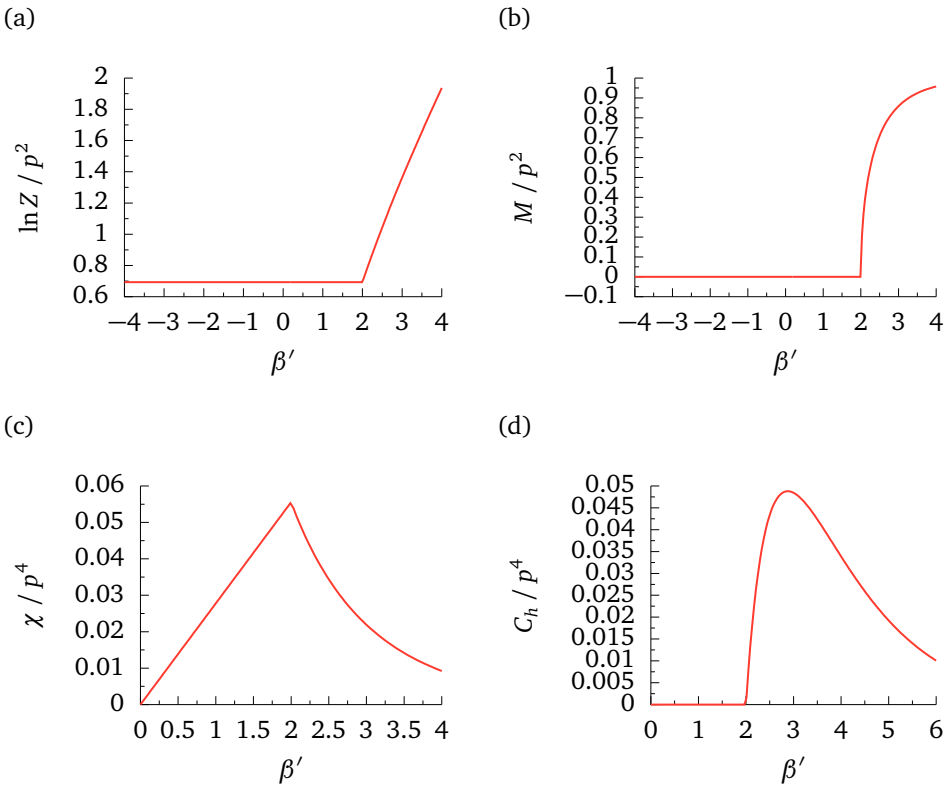

Figure 3: Plot a) shows the logarithm of the mean field partition function, calculated in Equation 29. In plot b) the positive solution to the magnetization from the self consistency condition (32) is shown. The susceptibility derived from the mean field approximation is depicted in c), the heat capacity is shown in d). All the plots are rescaled, such that they show the correct quantity for any $\mathfrak{PK}^2_p$.

5.2 Cluster expansion

Again, the case with spins on the affine plane and without external field is considered. By using the following relation,

$$e^{\beta\sigma_i\sigma_j} = \frac{e^{\beta}+e^{-\beta}}{2} + \frac{e^{\beta}-e^{-\beta}}{2}\sigma_i\sigma_j = \cosh\beta\ (1+\tanh\beta\ \sigma_i\sigma_j) \tag{39}$$

the general partition function of the Ising Model (24) can be simplified as follows.

$$Z = \sum_{\omega} e^{\beta\sum_{<i,j>}\sigma_i\sigma_j} = \tag{40}$$

$$= (\cosh\beta)^m \sum_{\omega}\prod_{<i,j>}(1+\tanh\beta\ \sigma_i\sigma_j) \tag{41}$$

Where m denotes the number of neighbor pairs $< i, j >$. Thus the above product gives 2^m terms. Each factor $\tanh\beta\sigma_i\sigma_j$ in these terms can be thought of as an edge between the vertices i and j in G. Where G is the graph that consists of all the points that are occupied by spins as vertices, and the neighbor pairs as its edges.

We can further simplify the sum, by exploiting that terms with uneven powers σ^{p_i} cancel out, because $\sigma_i \in \{1,-1\}$, and the sum is over all possible configurations. Therefore it suffices to consider the terms with only even powers for all σ_i. These terms will contribute with a factor of two to the overall sum. In the picture of the graph this means, only clusters that contain each vertex an even number of times and no edge twice, contribute to the sum.

$$Z = 2^n \cdot (\cosh\beta)^m \cdot \left(1 + \sum_{\text{clusters}} (\tanh\beta)^{\text{length of cluster}}\right) \tag{42}$$

With n the number of vertices in the graph, i.e. the number of spins in the system. So if we can compute the number of clusters with l nodes in G we have an exact expression for the partition function.

For the two-dimensional hypercubic lattice, this has been achieved by the means of considering circuits instead of clusters (See appendix B in [25]). A circuit is a sequence of adjacent vertices, where vertices may repeat, but no edge is traversed twice, with the same start and end vertex. Even if a way was found to enumerate circuits of a given length, the 'degeneracy' of a cluster, i.e. the number of circuits that cover the cluster is rather difficult to obtain. In fact, enumerating the number of Eulerian circuits, i.e. those circuits that contain each edge in the cluster, has been proven to be $\#P$-complete for a general undirected graph (in this case, the cluster subgraph) by Brightwell and Winkler [5]. However, in the particular case of a flat space (Equation 14) there might be a way to exploit the symmetry of the problem in order to at least calculate the first few coefficients in Equation 42.

This is often referred to as high-temperature expansion and extensive studies for conventional lattice structures have been performed by Domb, Skyes and others [8]. In

the high temperature approximation Equation 42 becomes:

$$Z = 2^n \cdot (\cosh\beta)^m \cdot \left(1 + \sum_l k_l (\tanh\beta)^l\right) \tag{43}$$

$$= 2^n \cdot (\cosh\beta)^m \cdot \left(1 + \sum_{l=1}^{r} k_l (\tanh\beta)^l + O(\beta^{r+1})\right) \tag{44}$$

$$= 2^n \cdot (\cosh\beta)^m \cdot \left(1 + \sum_{l=1}^{r} k_l (\tanh\beta)^l\right) + O(\beta^{r+1}) \tag{45}$$

Thus for high temperatures this gives a good approximation for the actual partition function.

For $l \in \{1, \ldots, 5\}$, the coefficients k_l are equal to the number of l-circuits on the graph of spins with the edges defined by the neighbor relations. For $l = 1, 2$, $k_l = 0$. For $l = 3$, k_3 is the number of triangles in the graph and can be computed as

$$B \coloneqq \left(A^2 - \operatorname{diag}\left(A^2\right)\right) \tag{46}$$

$$k_3 = \frac{1}{6} \operatorname{tr}(B \cdot A) \tag{47}$$

with A the adjacency matrix of the graph. For k_4 we consider open 2-*paths*, two distinct edges, that share a vertex. From the number of two consecutive open 2-paths, one has to subtract the number of consecutive open 2-paths that are not quadrilaterals, namely if both of them are identical.

$$k_4 = \frac{1}{8}\left(\operatorname{tr}\left(B^2\right) - n \cdot d \cdot (d-1)\right) \tag{48}$$

where $d = 2 \cdot (p-1)$ denotes the degree of the regular graph and $n = p^2$ the number of vertices. For k_5, C defines the matrix of open 3-paths. The number of degenerate pentagons (see Figure 4 for illustration) has to be subtracted from the trace of the composed open 2 and 3-path matrices.

$$C \coloneqq B \cdot A - \operatorname{diag}(B \cdot A) - (d-1) \cdot A \tag{49}$$

$$k_5 = \frac{1}{10}\left(\operatorname{tr}(C \cdot B) - 4 \cdot 3 \cdot k_3 \cdot (d-2)\right) \tag{50}$$

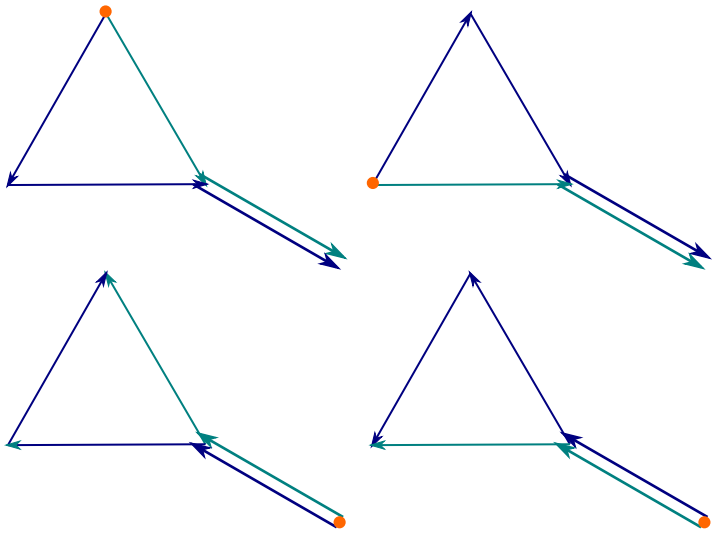

Figure 4: Possible combinations of an open 2-path and an open 3-path to form a given degenerate pentagon.

The numerical coefficients computed with the method described above are listed in Table 2 in Appendix A. A comparison with the exact solution for $\mathfrak{P}\mathbb{K}_5^2$ (Figure 5) shows that while the expansion suitably approximates the exact partition function for low β, the determined coefficients are not sufficient to extract any critical behavior (see Figure 6).

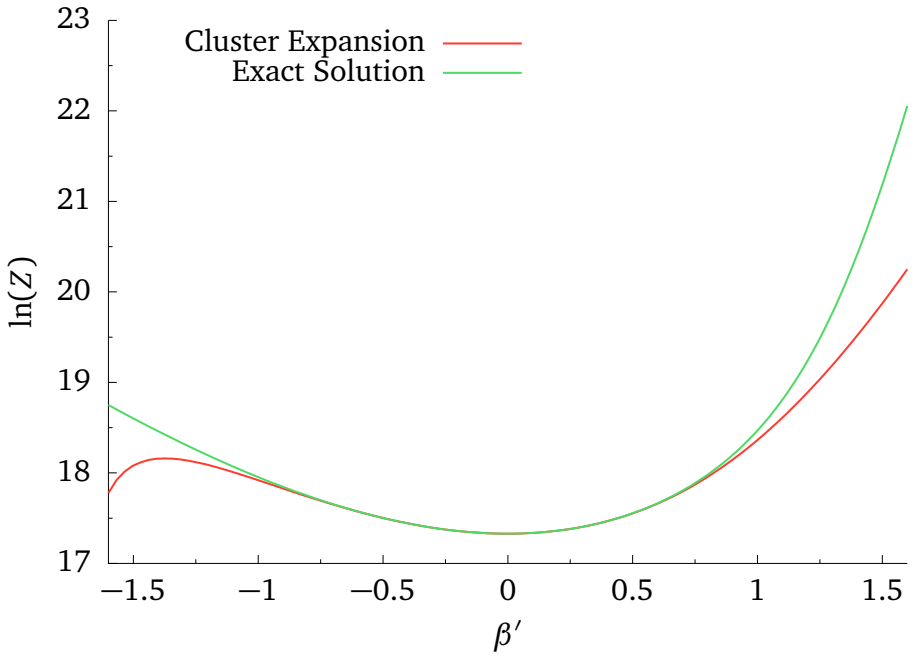

Figure 5: Approximate partition function obtained by high temperature expansion for $\mathfrak{P}\mathbb{K}_5^2$. In the region around $\beta' = 0$ the approximate partition function fits the exact one quite well.

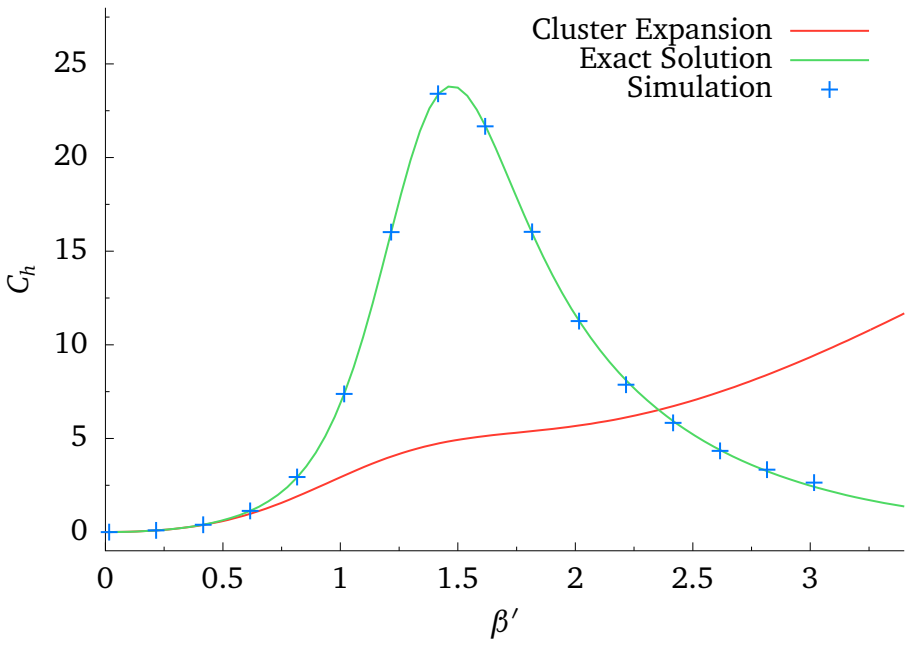

Figure 6: Approximate specific heat obtained by high temperature expansion for $\mathfrak{P}\mathbb{K}_5^2$ compared to the exact solution and Monte Carlo simulation. Although the expansion result shows the correct trend for $\beta' \lesssim 1$, it completely fails to reproduce the exact solution for larger β'.

For higher orders the numerics get arbitrarily complicated. A possible way to computationally push this idea further would be the use of general adjacency matrices $A(x)$, where each edge is assigned a symbol x_i. At some point in an algorithm that uses these general adjacency matrices, a check must be performed to ensure that only walks with the desired properties are considered. This idea has successfully been applied by Ponstein to the problem of enumerating simple cycles [22]. He found a rather efficient way to perform this check for simple cycles. Unfortunately no efficient generalization of this algorithm was found in the course of this thesis.

The vectorspace of all Eulerian subgraphs, the cycle space, provides an interesting perspective on the problem. A subgraph is called Eulerian if and only if every vertex in it has even degree. This is exactly the structure that has to be enumerated for the high temperature expansion. These subgraphs can be given a vectorspace structure over the field $\mathbb{K}_2$ with the symmetric difference. It can be shown that the vectorspace has the dimension $m-n+c$, where c is the number of connected components, so in this case $c = 1$. A corollary of this result is that the total number of Eulerian subgraphs is equal to 2^{m-n+1}, a useful criterion for verifying that a given set of expansion coefficients is correct. Algorithms based on the cycle space have been developed to enumerate simple cycles [23], but were not further considered in this thesis.

Another approach to this problem is considering a digraph, with each edge in the former graph replaced by two directed edges. The advantage is that the line graph, the graph whose points represent lines in the underlying graph and whose lines represent

adjacency of lines in the underlying graph, has some nice properties, as explained in [7]. For example the problem of enumerating Eulerian circuits that is $\#P$-complete for undirected graphs has a closed form solution through applying a combination of the BEST-Theorem [26] and the matrix-tree-theorem for undirected graphs.

A last deterministic approach was the direct application of tree search algorithms to constructively find the expansion coefficients. Unfortunately no improvement in time complexity over a direct brute force approach, that simply sums up all the terms in Equation 24 was achieved.

Finally, since a feasible deterministic algorithm seems rather hard to find, a naive randomization was implemented, using rejection sampling. But obviously, the ratio of Eulerian subgraphs to total subgraphs is with

$$\frac{2^{m-n+1}}{2^m} = 2^{1-n} = 2^{1-p^2} \tag{51}$$

far too small for this method to succeed. There might be better randomized algorithms that provide sharp approximations for the expansion coefficients, a result in that direction are the Kotzig transformations [14], but finding such an algorithm for the present problem is far beyond the scope of this thesis.

More advanced high temperature expansion methods can be found in [8]. The present analysis of the Ising Model on finite projective spaces will be continued by means of Monte Carlo simulation.

6 Monte Carlo Simulation

6.1 Description of the method

6.1.1 Metropolis

For the simulation, an implementation of the Metropolis Algorithm [18] in the Mocasinns Framework by Benedikt Krüger and Johannes F. Knauf [15], was used. The Metropolis Algorithm choses a state σ's probability according to the Boltzmann probability

$$P_{\text{Metropolis}} = \exp\left(-\beta' E[\sigma]\right) \tag{52}$$

Starting from a state σ^1, the Algorithm picks a random spin σ_i to be flipped. The new state, with σ_i flipped is called σ^2. The Metropolis acceptance probabilities are

$$p_A(\sigma^1 \to \sigma^2) = \begin{cases} 1 & \text{if } \Delta E \leq 0 \\ \exp(-\beta' \Delta E) & \text{if } \Delta E > 0 \end{cases} \tag{53}$$

The canonical average of an observable Q can be calculated by taking the arithmetic mean of the observable at each state.

$$\langle Q \rangle = \frac{1}{k} \sum_{i=1}^{k} Q(\sigma_i) \tag{54}$$

6.1.2 Choice of parameters

The spins are initialized in a highly ordered state. In order to compensate for this, the system is given some time to equilibrate before the actual measurement starts. In order to estimate how many Monte Carlo steps are required for the system to reach equilibrium, the time evolution of the energy, depicted in Figure 7a, was used. To be safe and because the computational cost of the first steps is rather low, the first 100 000 to 1 000 000 steps were not recorded for most measurements, depending on the field order.

Because each Monte Carlo step flips only one spin, making a measurement each step, would yield correlated results. Therefore, only after every n steps, a value for the observable is recorded. In order to determine a suitable number of steps between two measurements, the autocorrelation of sequential energies in the Monte Carlo simulation was selected as a criterion. This autocorrelation for several system sizes is shown in Figure 7b. The steps between measurements were chosen for each field order such that the correlation between two consecutive measurements was low.

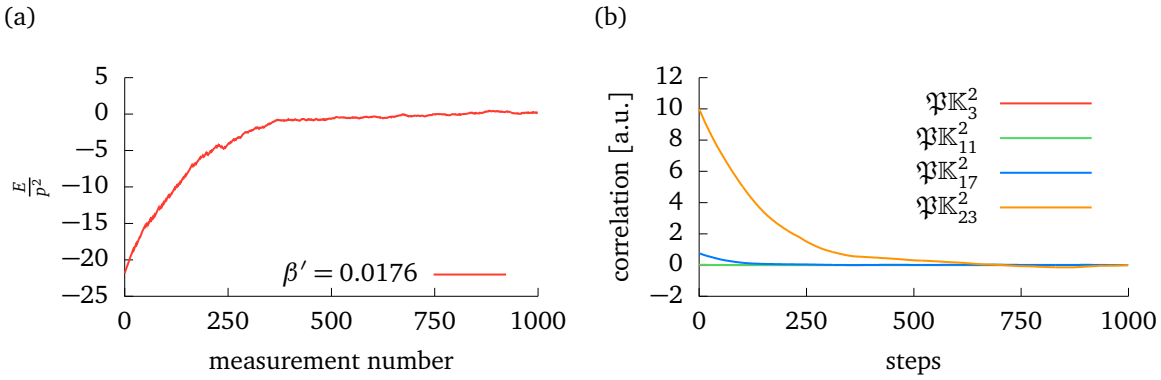

Figure 7: In Figure a), the energy development over time of $\mathfrak{PK}^2_{23}$ is shown. The system is initialized in a highly symmetric state and successively reaches thermal equilibration. The autocorrelation over time of the Simulation results is shown in b).

6.1.3 Susceptibility and heat capacity

Both the heat capacity and the susceptibility are calculated by means of the variance of the energy or magnetization.

$$\begin{aligned} C_V &= \frac{\partial E}{\partial T} = \frac{\beta'}{T}\frac{\partial^2 \ln Z}{\partial \beta'^2} = \frac{\beta'}{T}\frac{\partial}{\partial \beta'}\left(\frac{1}{Z}\frac{\partial Z}{\partial \beta'}\right) = \\ &= \frac{\beta'}{T}\cdot\left[\frac{1}{Z}\frac{\partial^2 Z}{\partial \beta'^2} - \frac{1}{Z^2}\left(\frac{\partial Z}{\partial \beta'}\right)^2\right] = \frac{\beta'}{T}\cdot\left[\langle E^2\rangle - \langle E\rangle^2\right] = \\ &= \beta'^2\cdot\left[\langle E^2\rangle - \langle E\rangle^2\right] \quad \text{for } k_B = 1 \end{aligned} \tag{55}$$

$$\chi = \frac{\partial M}{\partial T} = \beta'\cdot\left[\langle M^2\rangle - \langle M\rangle^2\right] \tag{56}$$

In case of the heat capacity, Equation 55 was directly used in the simulation. For the susceptibility, the situation is a little more complicated. While for an infinite lattice, both $\langle M\rangle$ and $\langle |M|\rangle$ are order parameters, for finite spin systems, $\langle M\rangle \equiv 0$. At a given temperature, two values for the overall magnetization are likely, one that is negative and one that is positive. In finite systems, there is a non-zero probability for a transition from one of these states towards the other. Therefore in the region slightly below the Curie temperature, the simulation fluctuates between those two states, resulting in an overall zero magnetization. Whereas for even lower temperatures and finite simulations, the system will transition to a broken-symmetry state (see Figure 10). These conditions are unfavorable for extracting the critical behavior near the Curie temperature.

One possible remedy is to prepare the system in an external magnetic field. Only then, the magnetic field will be lowered to zero, with the hope that the system will remain in the chosen symmetry-broken state. Another option is the introduction of a fixed spin. By simply keeping one spin on the lattice in a fixed configuration, the overall symmetry is broken and one of the parities is favored by the system, thus leading to

$\langle M \rangle \not\equiv 0$. While for small system sizes this method works well, for larger systems, the effect of the single spin becomes negligible and fluctuations dominate.

On the other hand $\langle |M| \rangle > 0$ for finite systems. So $\langle |M| \rangle$ is strictly speaking not a real order parameter. Because it is close to zero in the symmetric phase, it still serves as a usable order parameter for this simulation. We define

$$\chi' = \beta' \cdot \left[\langle M^2 \rangle - \langle |M| \rangle^2 \right] \tag{57}$$

Thereby we can avoid fluctuations, and get non-zero magnetization averages for temperatures around the Curie point. Thus, χ' is not exactly the theoretical susceptibility χ, but has the same scaling behavior and only varies by a constant factor above the Curie temperature [13]. Since we are only interested in scaling behavior, this modification is viable.

6.2 Results for affine spin configuration

6.2.1 Energy

One of the principal observables that were analyzed in the simulation was the energy and the corresponding heat capacity that was derived from it.

Like before, in the mean field approximation, the pseudo-critical temperature appears to be inversely proportional to the number of neighbors per spin (see Figure 8). So the choice of β' in Equation 38 is chosen for the affine simulation results as well. The energy itself scales with the number of neighbor pairs $p^2(p-1)$, as to be expected from the Hamiltonian (Equation 23).

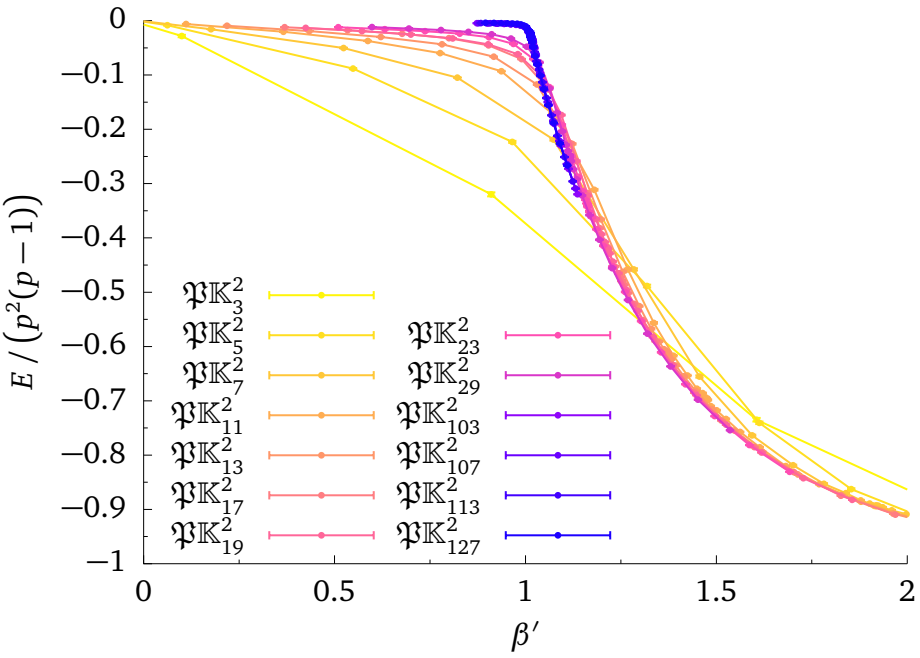

Figure 8: Simulated energy for different system sizes

As can be seen in Figure 6 and Figure 9, the numerical results fit the exact solution for low field orders calculated in section 4 very well. Although extensive unit testing was used to test the implementation, this important result underlines the overall reliability of the method.

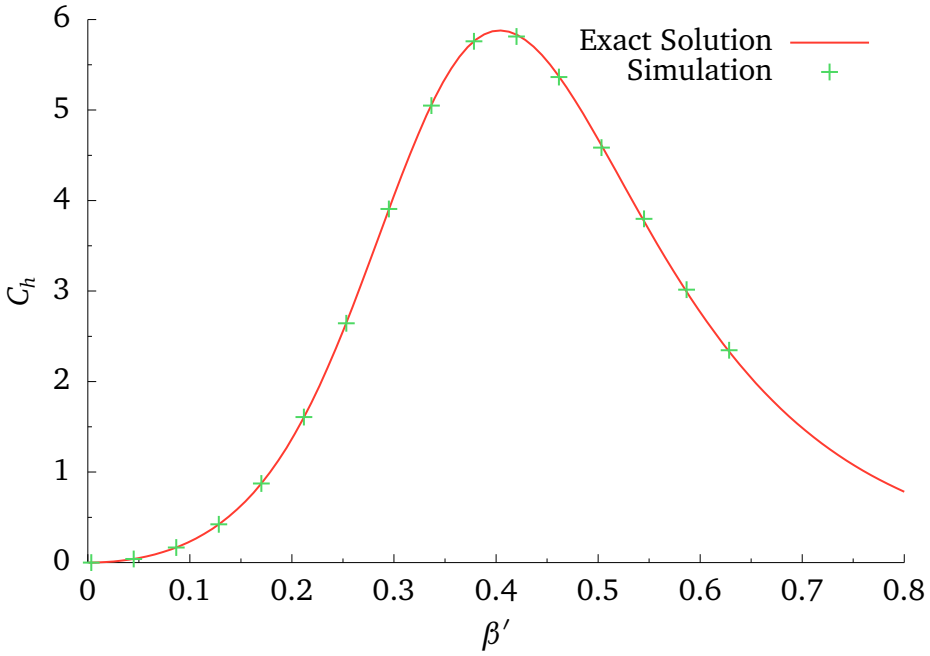

Figure 9: Comparison of exact and numerical heat capacity for $\mathfrak{P}\mathbb{K}_3^2$

6.2.2 Magnetization

The other main observable that was analyzed is the magnetization, because it serves as an order parameter of the Ising Model.

In the regions of high absolute external field, or high temperature, the numerically computed magnetization is a good approximation of its exact value. For temperatures below the Curie temperature and close to no external field however, there is spontaneous symmetry breaking. Therefore in simulations with finite samples, the simulated magnetization is unlikely to meet the theoretical zero (see Figure 10).

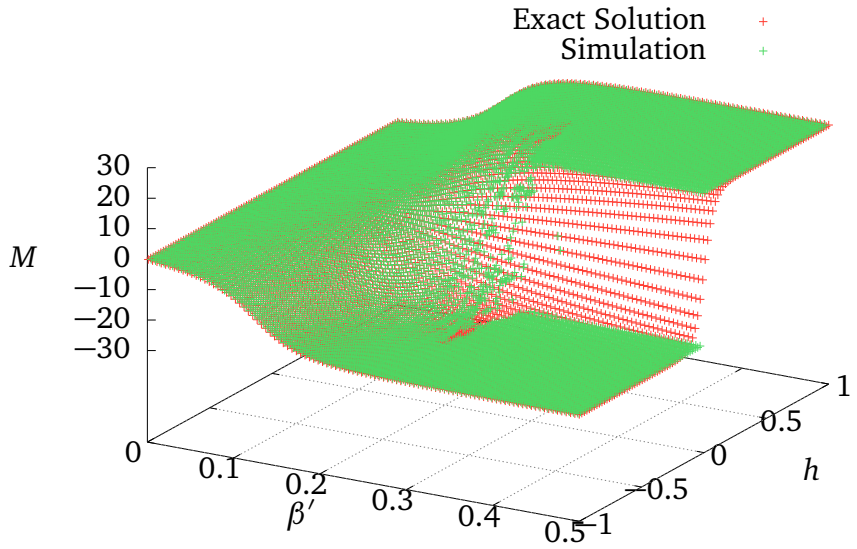

Figure 10: Exact and numerical magnetization over β' and h

As discussed previously in subsubsection 6.1.3, several variations of the magnetization have been considered as candidate order parameters.

The magnetization where one spin of the system is fixed to +1 in the simulation is shown in Figure 11. It can be seen, that for lower field orders, this modification has the desired effect. For higher field orders, the effect of a single spin on the whole system becomes increasingly weaker, to the point where the system favors the symmetric phase of negative pairity (here for $\mathfrak{PK}^2_{113}, \mathfrak{PK}^2_{117}, \mathfrak{PK}^2_{401}$). For some intermediate sized systems ($\mathfrak{PK}^2_{11}, \mathfrak{PK}^2_{13}, \mathfrak{PK}^2_{17}, \mathfrak{PK}^2_{19}$), the fluctuations between the two symmetric states lead to less precise and less accurate results. The introduction of a fixed spin has thus simply shifted the problem towards higher field orders.

The results for the absolute magnetization are depicted in Figure 11. Here, the problems in the symmetric phase are successfully evaded. In the symmetry broken phase however, the absolute magnetization is larger than the magnetization itself . For higher field orders, the magnetization in the symmetry broken phase rapidly decreases to near zero. This tradeoff for higher overall precision but less accuracy in the symmetry broken phase was chosen over the fixed spin solution.

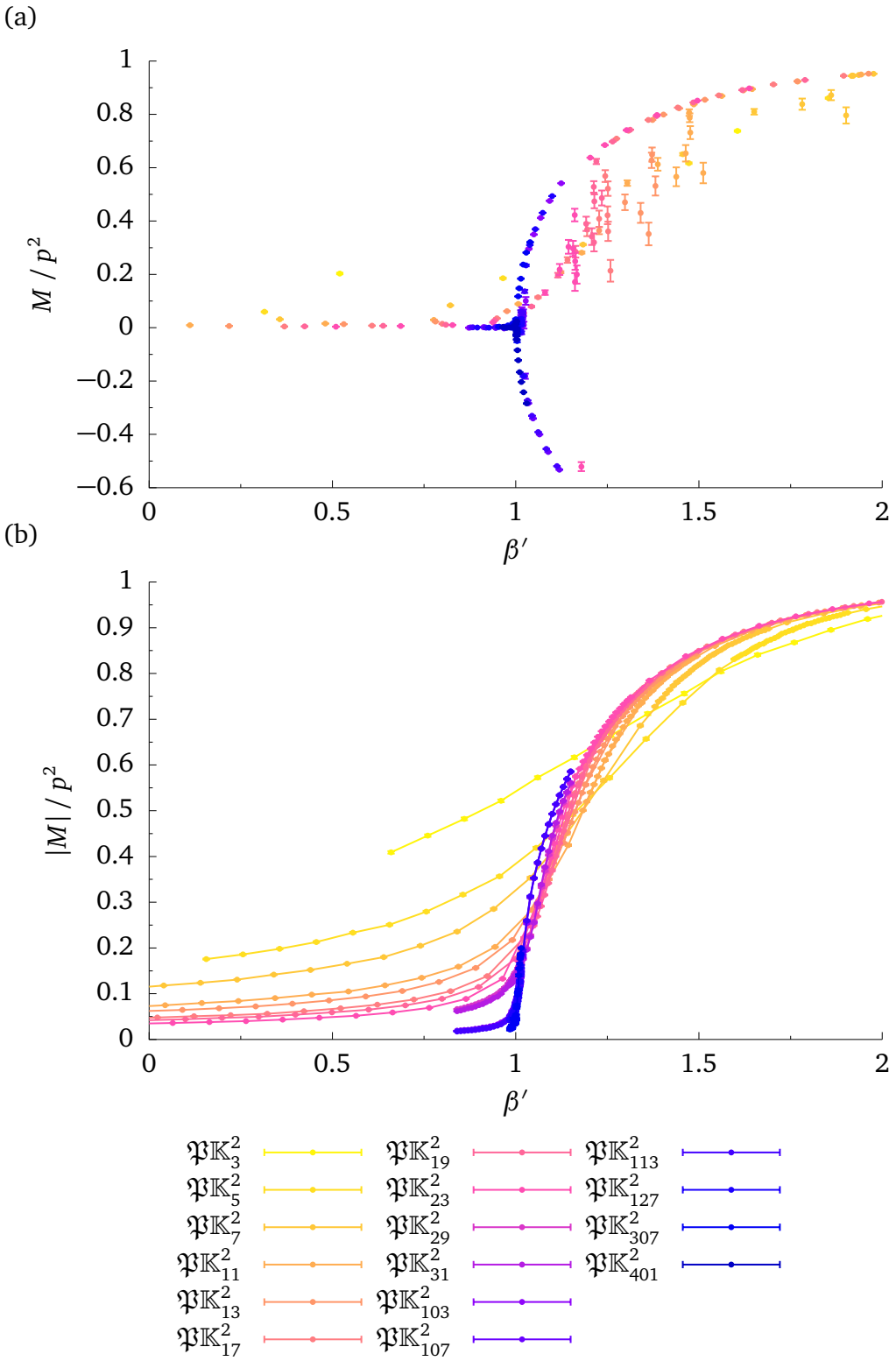

Figure 11: Figure a) shows the magnetization where one spin was fixed at +1 during the simulation. Figure b) shows the absolute magnetization as alternative order parameter. The legend applies to both plots.

6.2.3 Critical exponents

On a finite lattice, there is only a finite number of degrees of freedom and all the observables we consider are analytic. In order to learn more about the underlying geometry, it is of particular interest to investigate the critical behavior of phase transitions that occur for infinite systems. Finite size scaling offers a method to extrapolate the extremal behavior of finite systems to determine the infinite divergence critical exponents. In the following chapters two methods of finite size scaling are applied: In paragraph 6.2.3.1 an indirect method developed by Binder and in paragraph 6.2.3.2 direct finite size scaling via extrapolation.

6.2.3.1 Binder cumulant The critical point of an Ising system, can be determined from simulations with finite system sizes, via the use of Binder cumulants [2]. This method is often more accurate than a direct fit to the position of the susceptibility maxima, because finite size effects are reduced [13].

The fourth order *Binder cumulant* is defined as

$$U_L = 1 - \frac{\langle M^4 \rangle}{3\langle M^2 \rangle^2} \tag{58}$$

U_L has the following behavior for $L \to \infty$:

$$U_L = \begin{cases} 0 + \mathcal{O}\left(\frac{1}{n}\right) & \text{for } \beta' < \beta'_{\text{crit}} \\ \frac{2}{3} + \mathcal{O}\left(\frac{1}{n}\right) & \text{for } \beta' > \beta'_{\text{crit}} \\ U_L^\star & \text{for } \beta' = \beta'_{\text{crit}} \end{cases} \tag{59}$$

The Binder cumulants for finite system sizes are thus expected to intersect at the critical point.

The results of the simulated values for U_L are depicted in Figure 12a. In order to determine the intersection points for several system sizes, the ratios of a hyperbolic tangent fit are inspected in Figure 12b and β'_{crit} was determined as

$$\beta'_{\text{crit}} = 0.999 \pm 0.002 \tag{60}$$

The ratios selected in Figure 12b are arbitrary and were chosen, because some of the hyperbolic tangents come very close to each other at $\beta' \approx 1$, but do not intersect.

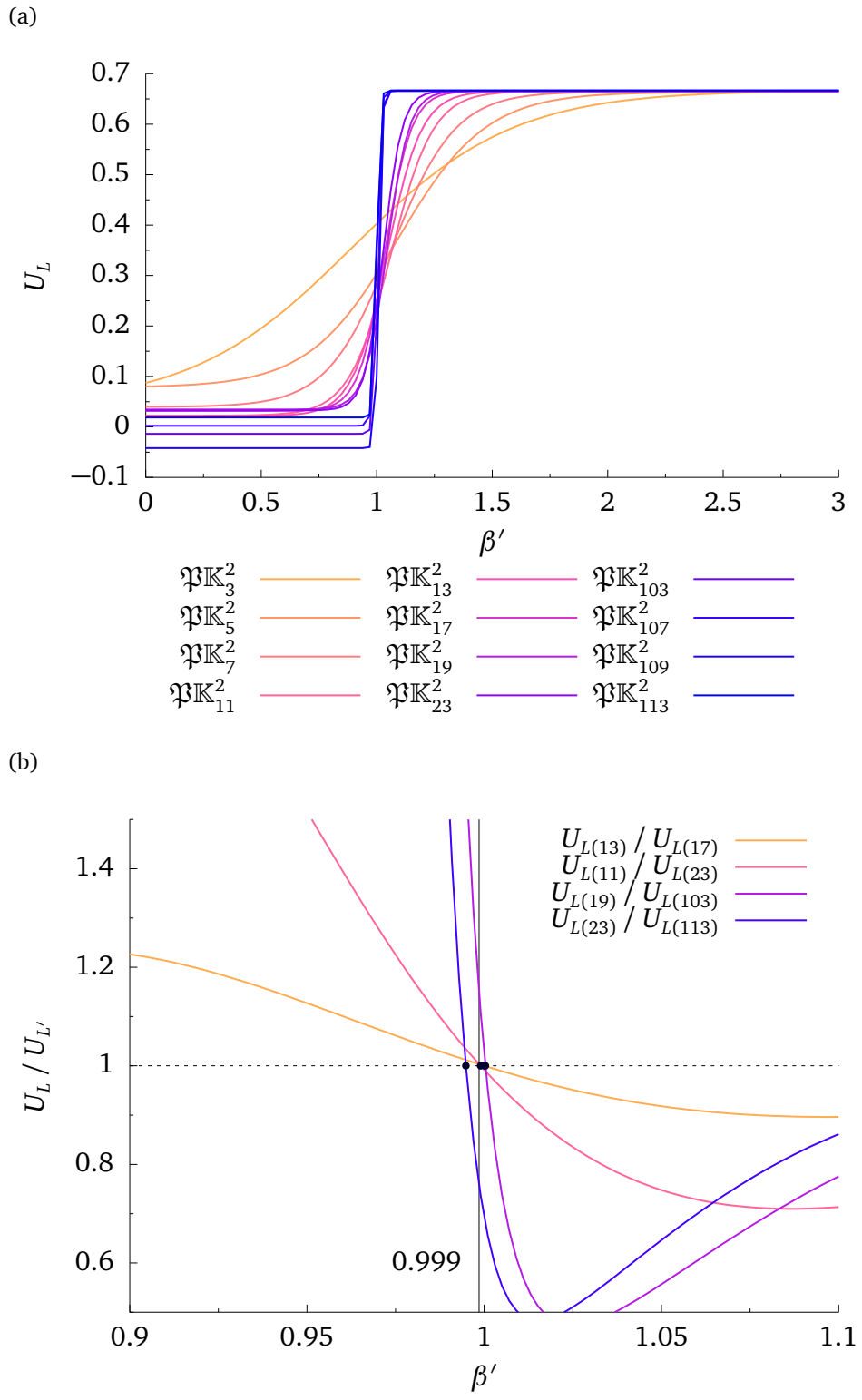

Figure 12: Figure a) shows the simulated Binder cumulant U_L for several field orders and a tanh fit to the data. The ratio between several of these fits is shown in graph b) and the respective intersection points are marked.

6.2.3.2 Finite size scaling The most important critical exponents for the Ising model are

$$\xi \propto |\tau|^{-\nu} \tag{61}$$
$$M \propto (\tau)^{\beta} \tag{62}$$
$$C_h \propto |\tau|^{-\alpha} \tag{63}$$
$$\chi \propto |\tau|^{-\gamma} \tag{64}$$

where $\tau := \frac{1}{\beta'} - \frac{1}{\beta'_c}$ and ξ the correlation length. For simplicity, we assume the critical exponents α, γ, ν to be the same above and below the critical temperature, although recent studies have shown that this is not necessarily always the case [16].

For a finite projective space $\mathfrak{P}\mathbb{K}^2_p$ with spins on the affine plane, the system is already effectively ordered at the correlation length $\xi \approx L(p)$, where L is the system size as a function of the field order p. For now we will assume $L \propto p$. Therefore, finite systems show a pseudo-critical point when

$$\left(\beta'_c(\infty) - \beta'_c(p)\right)^{-\nu} \approx L(p) \propto p \quad \Rightarrow \quad \beta'_c(p) = \beta'_c(\infty) - \text{const} \cdot p^{-\frac{1}{\nu}} \tag{65}$$

We assume the modified susceptibility $\chi' \propto |\tau|^{-\gamma}$ to peak at the pseudo-critical point $\beta'_c(p)$, and the maximum should be proportional to

$$\chi'_{\max} \propto \left(\beta'_c(p) - \beta'_c(\infty)\right)^{-\gamma} \propto p^{\frac{\gamma}{\nu}} \tag{66}$$

The argument for the heat capacity C_h is the same, but the susceptibility was chosen because from the square lattice Ising model we expect α to be much smaller than γ and thus it would be harder to obtain ν. For that reason, logarithmic corrections are not negligible anymore [13] and one would expect $C_h \propto C_0 \ln p$, supposing $\alpha = 0$. The numerical simulations support that hypothesis (see Figure 13a for a $C_0 \ln p$ fit to the maxima of C_h).

$$C_0 = 0.549 \pm 0.006 \tag{67}$$

The critical exponents can now be estimated by a power law fit of Equation 65 and Equation 66 to the simulated data as shown in Figure 13b and Figure 13c. This yields

$$\beta'_{\text{crit}} = 1.0009 \pm 0.0005 \tag{68}$$
$$\nu = 0.996 \pm 0.003 \tag{69}$$
$$\frac{\gamma}{\nu} = 2.08 \pm 0.05 \tag{70}$$
$$\alpha \approx 0 \tag{71}$$

The resulting value for β'_{crit} is compatible with the one obtained via the use of the Binder cumulant in Equation 60.

In order to determine the critical exponent β, the following scaling relation is applied:

$$\beta \cdot (\delta - 1) = \gamma \tag{72}$$

with δ the critical exponent for the field's dependance on the magnetization

$$H \propto M^{\delta} \tag{73}$$

at the critical temperature. Garcia et. al. [9] use a direct power law fit to the Magnetization to extract δ^{-1}. The same procedure is applied in this context in Figure 13d.

$$\gamma = \nu \cdot \frac{\gamma}{\nu} = 2.07 \pm 0.05 \tag{74}$$

$$\delta = 3.036 \pm 0.008 \tag{75}$$

$$\beta = \frac{\gamma}{\delta - 1} = 1.02 \pm 0.02 \tag{76}$$

Please note that due to the use of the absolute magnetization, the fit is done for relatively high values for h. This is strictly speaking not necessarily a good approximation for δ near the critical point. Therefore the error for δ, that results from the fit is an underestimation.

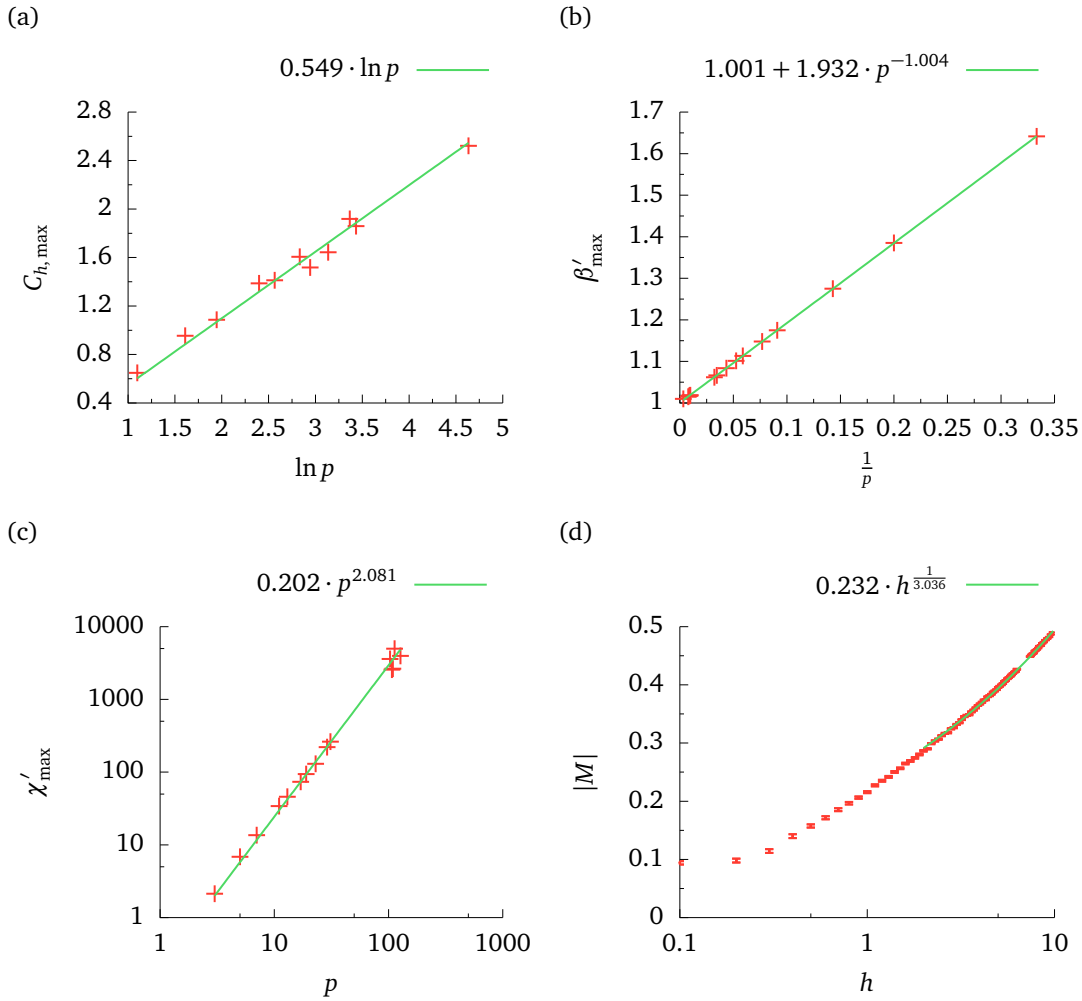

Figure 13: This Figure shows, how finite size scaling was applied, to extract the critical exponents. In a) the maxima of the simulated heat capcity for several system sizes is shown with a $C_0 \ln(p)$ fit. The position in terms of β' of the susceptibility χ' maxima over $\frac{1}{p}$ is depicted in b). As described in Equation 65 an exponential fit was made to determine β'_{crit} and $\frac{1}{\nu}$. In Figure c), Equation 66 is fitted to the the actual maximum values of the susceptibility χ', obtained via Monte Carlo simulation. Figure d) shows the external field dependance of the absolute magnetization for $\mathfrak{PK}^2_{103}$. The critical exponent δ is estimated via relation 73.

6.2.3.3 Mean field universality class With $\frac{\gamma}{\nu}, \alpha, \delta$ corresponding to the mean field universality class, one would expect $\nu \approx \frac{1}{2}$ accordingly, but roughly twice the mean field value is obtained numerically (Equation 68). Earlier, the naive assumption was made that the system size $L \propto p$, like for the hypercubic lattice.

The numerical results indicate, that a notion of system size, where $L \propto \sqrt{p}$ is more appropriate than $L \propto p$, because the values obtained from the simulation would agree with the mean field universality class exponents:

	System size $\propto$ p	**System size $\propto \sqrt{\text{p}}$**	**Mean field**
ν	0.996 ± 0.003	0.498 ± 0.002	$\frac{1}{2}$
γ	2.07 ± 0.05	1.04 ± 0.03	1
β	1.02 ± 0.02	0.51 ± 0.01	$\frac{1}{2}$

Table 1: Critical exponents

This result leads to the question, of how exactly the system size is defined.

In the hypercubic lattice, the Kadanoff construction [25], sometimes also referred to as coarse graining, gives an interpretation to the system size. For the neighbor structure of finite projective spaces it breaks down, because a choice of clusters with a surface to volume ratio $\ll 1$ is not really possible, especially for the limiting case of infinitely large p.

One plausible candidate for the system size, as it is used in Equation 65, is the graph diameter. For the hypercubic case, the graph diameter is equal to the lattice length. A hint that for the graphs induced by biquadric fields, this is not the case, is Bollobás' and Vega's conjecture [3]. It indicates that the diameter of a random regular graph with p^2 nodes and of degree $2 \cdot (p-1)$ is

$$\lim_{p\to\infty} d(G_{\text{random}}(p)) \approx \lim_{p\to\infty} \frac{\log\left(\frac{2p^2\log(p)}{p-1}\right)}{\log(2p-3)} + 2 = 3 \tag{77}$$

One could argue that the specific graphs induced by the biquadric field might behave differently from the random graph. Given the behavior for field orders $p < 100$ (Figure 14) it seems as if the diameter doesn't grow significantly with the field order.

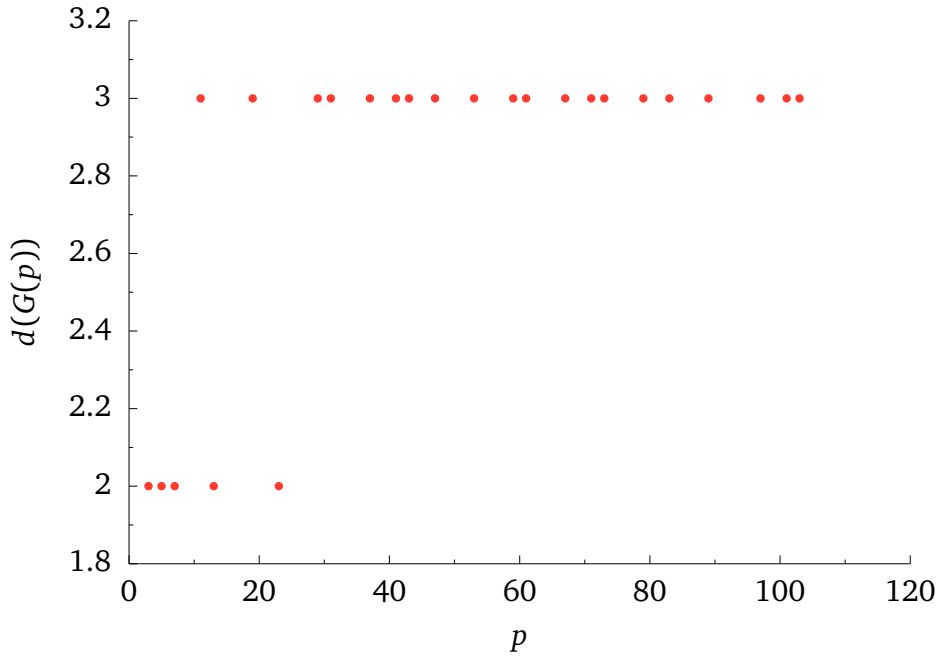

Figure 14: Diameter of affine neighborhood graph over field order

6.2.3.4 Hyperscaling Another argument for the reconsideration of $L \propto p$ is the following:

If the exponents in the first column of Table 1 were correct, the system would not lie in the mean field universality class. So the system must have lower than upper critical dimensionality and the hyperscaling relation would hold.

$$d\nu = 2\beta + \gamma \tag{78}$$

with d the dimension of the projective space.

In order to determine the critical exponent β while using hyperscaling, the root mean squared of M can be studied. M_{rms} can be expressed as

$$M_{\text{rms}} = \sqrt{\left\langle \frac{\left(\sum_x \sigma_x\right)\left(\sum_y \sigma_y\right)}{n^2} \right\rangle} = \sqrt{\frac{1}{n^2}\sum_x \left(\sum_y \langle \sigma_x \sigma_y \rangle \right)}$$
$$\overset{\text{isotropy}}{\propto} \sqrt{\frac{1}{p^d}\sum_y \langle \sigma_x \sigma_y \rangle} \tag{79}$$

where d is the dimension that relates the system size L to the point number $n = L^d$. At the critical point, the correlation function on the two-dimensional square lattice has rotational symmetry [1]. While it is not obvious, how this and the following result by Kadanoff [12], can be generalized to the projective space, both are assumed as working hypothesis.

$$\langle \sigma_x \sigma_y \rangle = G(|x-y|) \propto r^{-(d-2+\eta)}, \quad r \to \infty \tag{80}$$

At the infinite volume critical temperature β'_{crit}, we can approximate the correlation function as follows

$$\sum_y \langle \sigma_x \sigma_y \rangle \propto \int_0^{\frac{L}{2}} \mathrm{d}r\, r^{d-1} G(r) \overset{(80)}{\propto} \int_0^{\frac{L}{2}} \mathrm{d}r\, r^{1-\eta} \propto L^{2-\eta} \tag{81}$$

With the scaling law $2-\eta = \frac{\gamma}{\nu}$ and hyperscaling (78) and the premise $L \propto p$, Equation 79 becomes

$$M_{\text{rms}} \propto \sqrt{p^{2-d-\eta}} = p^{-\frac{\beta}{\nu}} \tag{82}$$

The root mean squared magnetization was simulated for several field orders (see Figure 15) and the critical exponent β could be determined to

$$\beta = 0.510 \pm 0.010 \tag{83}$$

This value contradicts the previous findings for $L \propto p$ in the first column of Table 1 and is another indication that $L \propto p$ is incorrect. It is interesting however, that M_{rms} still grows exponentially with the field order, with an exponent close to the mean field critical exponent.
In the above argumentation, it is unclear, what the notion of 'distance' in Equation 81 is, for finite projective geometries. The observations in Figure 14 suggest, that the notion of 'distance' is distinct of the distance in a graph, defined by the shortest graph geodesic.

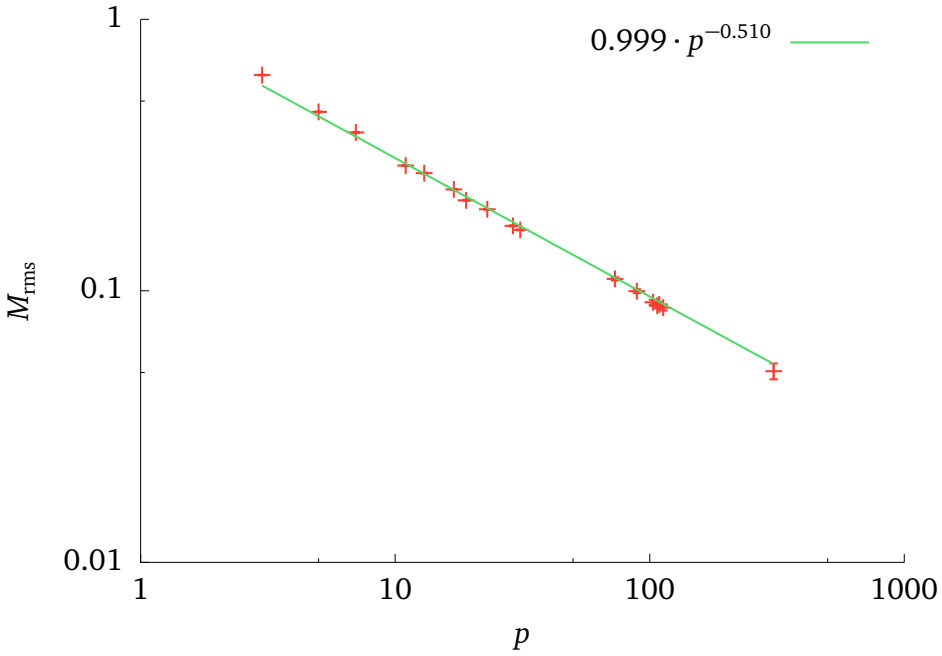

Figure 15: M_{rms} for $\beta'_{\text{crit}} = 1$

6.3 Results for hyperplane spin configuration

Additionally to the case where spins are placed only in the affine space $\mathfrak{AK}^2$, we investigate the situation with spins also on the line at infinity. In this case there is no unique coordination number, because the geometry is not isotropic anymore. With the Minkowski pre-metric, every spin in the affine plane has besides the $2 \cdot (p-1)$ neighbors in the affine plane also 2 neighbors on the line at infinity, namely:

$$\left\langle \begin{array}{c} 1 \\ 1 \\ 0 \end{array} \right\rangle \text{ and } \left\langle \begin{array}{c} -1 \\ 1 \\ 0 \end{array} \right\rangle \tag{84}$$

For the other spins at infinity, a different degenerate biquadric is introduced to define the neighborhood relations. In the case of a line at infinity any choice of biquadric leaves the spins at infinity with two neighbors each, plus the p^2 affine neighbors for $\left\langle \begin{array}{c} 1 \\ 1 \\ 0 \end{array} \right\rangle$ and $\left\langle \begin{array}{c} -1 \\ 1 \\ 0 \end{array} \right\rangle$. Therefore it is a priori not clear, how the physical observables scale with β and how β' should be defined for this case.

Possible candidates are the previous definition of β' for comparability of the results, the affine coordination number $2q$ or even something like a mean number of neighbors

$$\beta'_{\text{mean}} = 2 \cdot \frac{p^2 + p + 1}{p + 1} \tag{85}$$

The first two candidates only differ by a constant and will obviously result in the same scaling behavior. Of the two, only the previous β' with $2 \cdot (p-1)$ neighbors is considered.

6.3.0.1 Generalized mean field approximation Given the previous results for spins only on the affine plane, what to expect for the general case, where spins are also placed on the line at infinity? The Hamiltonian can now be written as

$$\mathscr{H}_{\mathfrak{PK}^2_p}(J, h=0) = \mathscr{H}_{\mathfrak{AK}}(J, h=0) + \mathscr{H}_{\mathfrak{AK}^2}(J, h=(\sigma_{\hat{q}^+_\infty} + \sigma_{\hat{q}^-_\infty})) \tag{86}$$

A first mean field type approximation can be made by essentially separating the line from the plane and only then feeding the mean values for $\sigma_{\hat{q}^+_\infty} + \sigma_{\hat{q}^-_\infty}$ into the plane Hamiltonian.

$$\langle \sigma_{\hat{q}^+_\infty} + \sigma_{\hat{q}^-_\infty} \rangle = 2 \cdot \langle \sigma \rangle = 0 \tag{87}$$

For the one-dimensional Ising chain with periodic boundary conditions. So that gives

$$\mathscr{H}_{\mathfrak{PK}^2_p}(J, h=0) \approx \mathscr{H}_{\mathfrak{AK}}(J, h=0) + \mathscr{H}_{\mathfrak{AK}^2}(J, h=0) \tag{88}$$

The second term being the previously studied Hamiltonian and the first one the one dimensional Ising Hamiltonian with periodic boundary conditions. The overall partition function will thus only differ by a factor of

$$Z_{\mathfrak{AK}} = 2^p (\cosh \beta)^p \cdot (1 + (\tanh \beta)^p) \tag{89}$$

from the affine plane partition function. A similar approximation of the same type is to consider the spins $\sigma_{\hat{q}^+_\infty} + \sigma_{\hat{q}^-_\infty}$ as assuming the mean magnetization of the affine plane, because they are connected to every single spin on the affine plane. This will give the following very similar partition function

$$Z_{\mathfrak{P}\mathbb{K}^2_p} \approx 2^{p-2}(\cosh\beta)^p \cdot (1 + (\tanh\beta)^p \cdot \langle\sigma_{\hat{q}^+_\infty}\rangle\langle\sigma_{\hat{q}^-_\infty}\rangle) \cdot Z_{\mathfrak{A}\mathbb{K}^2} = \tag{90}$$

$$= 2^{p-2}(\cosh\beta)^p \cdot (1 + (\tanh\beta)^p \cdot M^2_{\mathfrak{A}\mathbb{K}^2}) \cdot Z_{\mathfrak{A}\mathbb{K}^2} \tag{91}$$

with the affine specific magnetization $M_{\mathfrak{A}\mathbb{K}^2}$.

Both these approximations fail to reproduce the results obtained from the simulation. Exemplary the heat capacity is depicted in Figure 16. The approximation does not only differ from the absolute curves, also the scaling behavior with the system size does not match the simulation. This is a first indication that the spins at infinity change the critical exponents.

It is thus not sufficient to separate the line at infinity from the affine plane. It appears, that the connection through the line at infinity, gives rise to a fundamentally different topology.

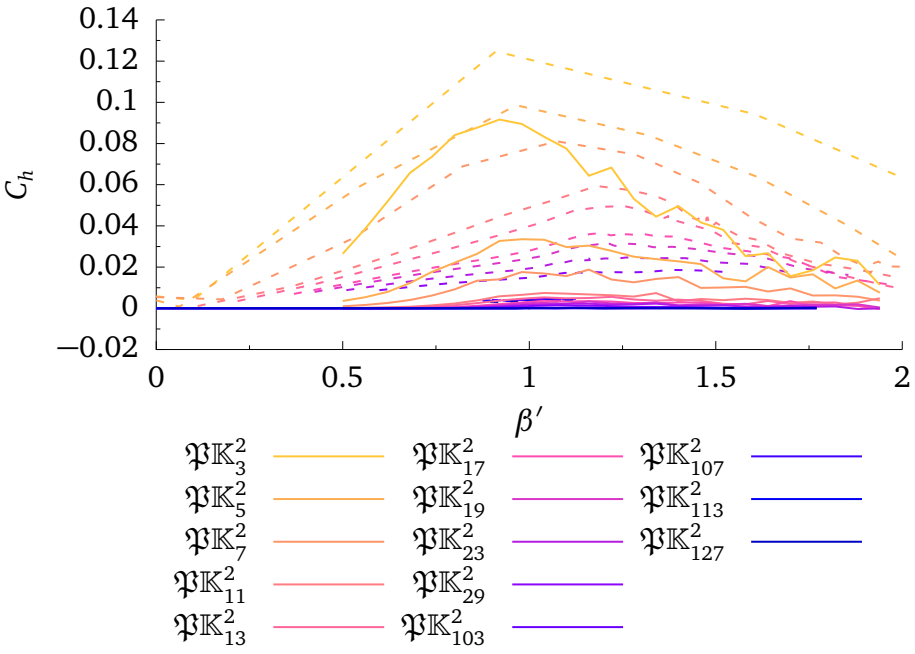

Figure 16: The expected heat capacity from the approximation in Equation 88 is drawn as dashed line. The simulation results for the heat capacity with spins at infinity are shown as full lines.

Because of the low expansion order achieved for the affine case, cluster expansion methods were not considered for the case with spins at infinity. Instead, the focus lies on a Monte Carlo analysis. The same methods as in subsubsection 6.2.3 are applied.

6.3.0.2 Simulation results With the Binder cumulant (Figure 17b and 17a), β'_{crit} could be determined to

$$\beta'_{\text{crit}} = 0.884 \pm 0.050 \tag{92}$$

$$\beta'_{\text{mean, crit}} = 0.820 \pm 0.040 \tag{93}$$

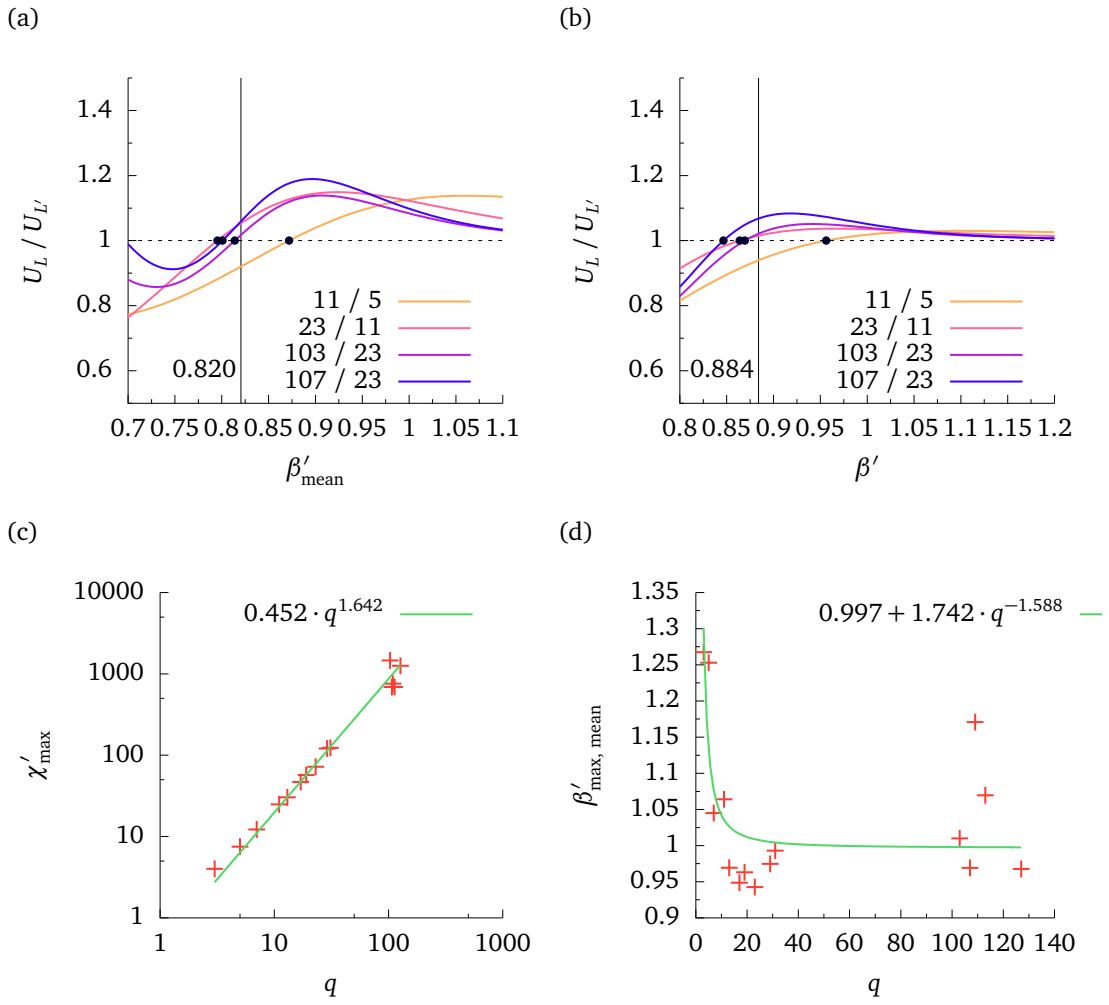

Figure 17: Figure a) and b) show the ratio of a tanh fit to the Binder cumulant for spins on the line at infinity. In Figure a), Equation 85 was used for scaling β, whereas in Figure b), the definition of β' for the case with spins exclusively on the affine plane, was used. Figure c) shows the dependence of the susceptibility χ' maxima on the field order. In Figure d) the positions of these maxima in terms of β'_{mean} is shown.

The individual values for β'_{mean} in Figure 17d do not agree with the critical inverse temperature obtained through the Binder cumulant. None of the individual values for β'_{mean} lies below 0.9, so a $\beta'_{\text{mean, crit}} = 0.820 \pm 0.040$ seems unlikely.

The values for β' agree a little bit better, but nevertheless, no reliable exponential fit could be made. The results for β' are better, because the system can, in first order, be

regarded as a disturbance of the affine case. The critical exponent δ was not determined, because of the high uncertainty in the value of β' and the sensitive dependance of δ thereof.

The ratio of the critical exponents $\frac{\gamma}{\nu}$ is obtained from the fit in Figure 17c.

$$\frac{\gamma}{\nu} = 1.64 \pm 0.07 \tag{94}$$

This value does not fit into any of the hypercubic Ising universality classes. Given the spread of the data in Figure 17d and the remaining question of how a system size should be defined in the case with spins at infinity, no definitive conclusions can be drawn.

7 Conclusion and Outlook

In the course of this thesis, evidence was found, that the critical behavior of the Ising Model on two-dimensional finite projective geometries, for spins on the affine plane only, corresponds to the mean field universality class. This result is most likely due to the number of neighbors being proportional to the field order. For field orders ≥ 3, the number of neighbors is greater or equal to the number of neighbors in the four-dimensional hypercubic Ising Model. The upper critical dimension for the hypercubic Ising Model is known to be four, where the dimension characterizes how many neighbors each site has. From this perspective, it is not surprising, that the mean field critical exponents hold in the case of finite projective geometries. Furthermore it has been found, that the notion of 'system size' has to be revisited for finite projective spaces. The numerical results indicate that such a system size should be proportional to the square root of the field order. The graph diameter as candidate for this system size was rejected. Therefore the question for a proper definition remains open. Related to this problem is the search for a definition of length, that can explain the exponential behavior of the root mean squared magnetization. In the future, definitions using a projectively invariant cross ratio, as proposed by Mecke [17], could be investigated.

It was also found that in the case where spins are also placed on the line at infinity, cannot simply be described by disjoint analysis of the affine plane and the line at infinity. The numerical results underline, that the situation is more complicated in that case and how sensitive the Ising Model is to its underlying geometry.

Considerable effort has been invested in the graphology of the high temperature expansion, but only the coefficients up to fifth order could be determined. The rapidly increasing number of neighbors with the field order, imposes difficulties in calculating the expansion coefficients. Therefore extrapolation methods like ratio methods or Padé approximants could not be applied reliably. The theory of high temperature expansion developed by Domb, Sykes and others [8] could be further transferred to finite projective geometries. Perhaps, the case with spins at infinity, can be understood better, with these expansion techniques.

In any case, the underlying topology and the behavior of the Ising Model are closely related and the study of one bares fruitful insights for the other. It is thus worthwhile to seek further answers to the questions raised in this thesis.

A Table of calculated high-temperature expansion coefficients

p	k_3	k_4	k_5
3	6	9	36
5	100	250	1320
7	196	1617	17052
11	2420	19965	235708
13	1352	35490	653016
19	17328	250173	5510304
23	0	436425	15013020
29	47096	1165626	49780472
31	76880	1888365	71925084
37	32856	3523806	185603544
41	134480	5143860	306802672
43	51772	7649313	370894608
47	0	10517049	624316416
53	0	16870854	1132903408
59	403796	22713525	2008481304
61	595360	28019130	2422549608
67	197516	41626497	3806528352
71	705740	57694245	5167004836
73	255792	58512420	5901888816
79	1298128	78617877	8954162412
83	0	97444905	11496804096
89	1394096	136969932	16545131328
97	602176	186524016	25275133248
101	2040200	215751150	31370931280

Table 2: High temperature expansion coefficients

References

[1] BARIEV, R. Z.: On the rotational symmetry of the spin-spin correlation function of the two-dimensional Ising model. In: *Physics Letters A* 55 (1976), Februar, Nr. 8, 456–458. http://dx.doi.org/10.1016/0375-9601(76)90219-X. – DOI 10.1016/0375–9601(76)90219–X. – ISSN 0375–9601

[2] BINDER, K.: Finite size scaling analysis of ising model block distribution functions. In: *Zeitschrift für Physik B Condensed Matter* 43 (1981), Juni, Nr. 2, 119–140. http://dx.doi.org/10.1007/BF01293604. – DOI 10.1007/BF01293604. – ISSN 0722–3277, 1431–584X

[3] BOLLOBÁS, Béla ; VEGA, W. Fernandez de l.: The diameter of random regular graphs. In: *Combinatorica* 2 (1982), Juni, Nr. 2, 125–134. http://dx.doi.org/10.1007/BF02579310. – DOI 10.1007/BF02579310. – ISSN 0209–9683, 1439–6912

[4] BOROS, George ; MOLL, Victor: *Irresistible Integrals: Symbolics, Analysis and Experiments in the Evaluation of Integrals*. 1 edition. Cambridge, UK ; New York : Cambridge University Press, 2004. – ISBN 978–0–521–79636–1

[5] BRIGHTWELL, Graham R. ; WINKLER, Peter: Note on Counting Eulerian Circuits. In: *CDAM research report series* LSE-CDAM-2004-12 (2004)

[6] CAMERON, Peter J.: *Projective and polar spaces*. University of London, Queen Mary and Westfield College, 1992

[7] CARTWRIGHT, Dorwin ; GLEASON, Terry C.: The number of paths and cycles in a digraph. In: *Psychometrika* 31 (1966), Juni, Nr. 2, 179–199. http://dx.doi.org/10.1007/BF02289506. – DOI 10.1007/BF02289506. – ISSN 0033–3123, 1860–0980

[8] DOMB, Cyril ; GREEN, Melville S. ; LEBOWITZ, Joel L.: *Phase transitions and critical phenomena*. Academic Press, 1989. – ISBN 978–0–12–220313–8. – Google-Books-ID: vp8mAAAAMAAJ

[9] GARCIA, Jorge ; GONZALO, Julio A. ; MARQUES, Manuel I.: Accurate Monte Carlo critical exponents for Ising lattices. In: *arXiv:cond-mat/0211270* (2002), November. http://arxiv.org/abs/cond-mat/0211270. – arXiv: cond-mat/0211270

[10] HIRSCHFELD, James William P.: *Projective geometries over finite fields*. Clarendon Press, 1979. – ISBN 978–0–19–853526–3. – Google-Books-ID: 3iiCAAAAIAAJ

[11] ISING, Ernst: Beitrag zur Theorie des Ferromagnetismus. In: *Zeitschrift für Physik* 31 (1925), S. 253–258

[12] KADANOFF, L.P.: Scaling Laws for Ising Models Near Tc. In: *Physics* 2 (1966), S. 263

[13] KOTZE, Jacques: Introduction to Monte Carlo methods for an Ising Model of a Ferromagnet. In: *arXiv:0803.0217 [cond-mat]* (2008), März. http://arxiv.org/abs/0803.0217. – arXiv: 0803.0217

[14] KOTZIG, Anton: Moves Without Forbidden Transitions in a Graph. In: *Matematický časopis* 18 (1968), Nr. 1, 76–80. http://eudml.org/doc/33972

[15] KRÜGER, Benedikt ; KNAUF, Johannes F.: *MOnte-CArlo-SImulations - Neat'N'Simple*. http://bkrueger.github.io/mocasinns/. Version: April 2016

[16] LÉONARD, F. ; DELAMOTTE, B.: Critical Exponents Can Be Different on the Two Sides of a Transition: A Generic Mechanism. In: *Physical Review Letters* 115 (2015), November, Nr. 20, 200601. http://dx.doi.org/10.1103/PhysRevLett.115.200601. – DOI 10.1103/PhysRevLett.115.200601

[17] MECKE, Klaus: Biquadrics configure finite projective geometry into a quantum spacetime. In: *EPL (Europhysics Letters)* 120 (2017), S. 10007

[18] METROPOLIS, Nicholas ; ROSENBLUTH, Arianna W. ; ROSENBLUTH, Marshall N. ; TELLER, Augusta H. ; TELLER, Edward: Equation of State Calculations by Fast Computing Machines. In: *The Journal of Chemical Physics* 21 (1953), Juni, Nr. 6, 1087–1092. http://dx.doi.org/10.1063/1.1699114. – DOI 10.1063/1.1699114. – ISSN 0021–9606

[19] ONSAGER, Lars: Crystal Statistics. I. A Two-Dimensional Model with an Order-Disorder Transition. In: *Phys. Rev.* 65 (1944), Februar, Nr. 3-4, 117–149. http://dx.doi.org/10.1103/PhysRev.65.117. – DOI 10.1103/PhysRev.65.117

[20] OSWALD VEBLEN ; JOHN WESLEY YOUNG: *Projective Geometry Vol I*. Ginn and Company, 1910 http://archive.org/details/projectivegeomet004116mbp

[21] OSWALD VEBLEN ; JOHN WESLEY YOUNG: *Projective Geometry Volume II*. Blasidell Publishing Company, 1946 http://archive.org/details/projectivegeomet028875mbp

[22] PONSTEIN, Jacob: Self-Avoiding Paths and the Adjacency Matrix of a Graph. In: *SIAM Journal on Applied Mathematics* Vol .14, No. 3 (1966), Mai, 600 – 609. http://links.jstor.org/sici?sici=0036-1399%28196605%2914%3A3%3C600%3ASPATAM%3E2.0.CO%3B2-E

[23] RAO, V. V. B. ; MURTI, V. G. K.: Enumeration of all circuits of a graph. In: *Proceedings of the IEEE* 57 (1969), April, Nr. 4, S. 700–701. http://dx.doi.org/10.1109/PROC.1969.7032. – DOI 10.1109/PROC.1969.7032. – ISSN 0018–9219

[24] SCHNEIDER, Bruce: *Applied Cryptography: Protocols, Algorithms, and Source Code in C*. Second Edition (2nd ed.). Wiley, 1996. – ISBN 978–0–471–11709–4

[25] STANLEY, Harry E.: *Introduction to Phase Transitions and Critical Phenomena*. First Edition. Oxford University Press, 1971 (Monographs on Physics). http://gen.lib.rus.ec/book/index.php?md5=BF04EFD59645091B5B787A9A45A42724. – ISBN 978–0–19–851257–8

[26] VAN AARDENNE-EHRENFEST, Tanja ; BRUIJN, Nicolaas G.: Circuits and trees in oriented linear graphs. In: *Simon Stevin* 28 (1951), S. 203–207

[27] WOESTIJNE, Christiaan Evert van d.: *Deterministic equation solving over finite fields*. Faculty of Mathematics and Natural Sciences, Leiden University, 2006 http://hdl.handle.net/1887/4392. – ISBN 978–90–90–20668–4

Danksagung

An dieser Stelle möche ich Prof. Dr. Klaus Mecke, dessen Ideen diese Arbeit überhaupt erst ermöglichten, aufrichtig danken. Unsere zahlreichen Gespräche halfen mir, Feinheiten der Theorie der Biquadrikfelder besser zu verstehen und gaben immer wieder Denkanstöße, die Eingang in die Arbeit fanden. Alexander Laska danke ich für die abschließende Durchsicht der Arbeit.

Erklärung

Hiermit versichere ich, dass ich die vorliegende Arbeit selbstständig verfasst und keine anderen als die angegebenen Quellen und Hilfsmittel benutzt habe, dass alle Stellen der Arbeit, die wörtlich oder sinngemäß aus anderen Quellen übernommen wurden, als solche kenntlich gemacht sind und dass die Arbeit in gleicher oder ähnlicher Form noch keiner Prüfungsbehörde vorgelegt wurde.

Erlangen, den 29. Juni 2018

Kai Klede